

**Transforming Energy Using Quantum Dots**

Journal:	<i>Energy & Environmental Science</i>
Manuscript ID	EE-REV-12-2019-003930.R2
Article Type:	Review Article
Date Submitted by the Author:	03-Mar-2020
Complete List of Authors:	Lu, Haipeng; National Renewable Energy Laboratory, Chemistry & Nanoscience Center Huang, Zhiyuan; National Renewable Energy Laboratory, Chemical and Nanoscience Center Martinez, Marissa; National Renewable Energy Laboratory, Chemical and Nanoscience Johnson, Justin; NREL, Luther, Joseph; National Renewable Energy Laboratory, Beard, Matthew; National Renewable Energy Laboratory, Chemical and Nanoscience

Transforming and directing the flow of energy from one form (e.g., sunlight, electricity, etc.) to other useful forms of energy (e.g., electricity, chemical bonds, light, etc.) in an efficient and controllable manner is critical to meet the increasing energy demands and build a sustainable society. In search of such energy mediators, colloidal semiconductor nanocrystals, or quantum dots (QDs) are promising building blocks for building and designing systems that can efficiently capture light and convert and direct that energy into other useful forms of energy. In this review article, we summarize recent advances using QDs in energy conversion architectures with the express goal of converting optical energy to other forms of energy, including electricity (i.e., photovoltaics), photons with different energies (i.e., photo up- or down-conversion), and chemical bonds (i.e., photocatalysis). The advantages of employing QDs over molecular chromophores in absorbing and then directing and converting optical energy are highlighted. Finally, we discuss ongoing challenges as well as unique opportunities associated with the use of QDs for transforming energy.

Transforming Energy Using Quantum Dots

Haipeng Lu,* Zhiyuan Huang, Marissa S. Martinez, Justin C. Johnson, Joseph M. Luther, Matthew C. Beard*

Chemistry & Nanoscience Center, National Renewable Energy Laboratory, Golden, Colorado 80401, United States

Corresponding Author

Haipeng Lu*: Haipeng.Lu@nrel.gov

Matthew C. Beard*: Matt.Beard@nrel.gov

ABSTRACT

Colloidal quantum dots (QDs) have emerged as versatile and efficient scaffolds to absorb light and then manipulate, direct, and convert that optical energy into other useful forms of energy. The QD characteristics (optical, electrical, physical) can be readily tuned via solution phase chemistries in order to affect the flow of energy, that was initially contained in the photons of light, using rational designs. Key parameters under control are the size and shape, internal composition (*e.g.*, alloys, core/shell heterostructures, semiconductor/metal interfaces), surface composition (ligand chemistries), and film composition (*e.g.*, QD-QD electronic coupling, bulk heterostructure formation, QD/biological interfaces). In this review, we summarize recent progress using QDs in energy conversion architectures with the express goal of converting optical energy to other forms of energy, including electricity, photons with different energies, and chemical bonds, *i.e.*, photovoltaics, photon up-or down-conversion, and photocatalytic process, respectively. The advantages of using QDs in absorbing and then directing and converting optical energy over molecular chromophores are highlighted. Finally, we discuss ongoing challenges and opportunities associated with using QDs for absorbing, manipulating and directing the flow of energy.

1. Introduction

Nature has established a mature and sustainable ecosystem to cycle energy between different forms. At the first trophic level, nature converts an external energy source, namely solar energy, to other forms of energy needed in the ecosystem and supports life. This process, thus, represents the most important step in the energy cycle. Designing artificial systems that can mimic nature to efficiently convert optical energy to other forms of energy can lead to the development of currently unimagined ways of producing energy to meet the increasing energy demand and thus build a sustainable society.

In search of such artificial systems, colloidal semiconductor nanocrystals, or quantum dots (QDs) are promising building blocks to design systems to capture light and convert that energy to other

useful forms. Because of the quantum confinement effect, the optical and electrical properties of colloidal QDs can be readily tuned by controlling their physical dimensions (size and shape) without the need to break and/or build chemical bonds (*e.g.*, their bandgap increases as the QD size decreases). The large absorption coefficients, in conjunction with broad and tunable absorption spectra, make QDs excellent solar absorbers. When combined with a metal contact (which may form a Schottky junction) or with another semiconductor, forming a heterostructure, photogenerated carriers produced in the QD layers can be separated, performing as photovoltaic devices. As such, QDs can be used to convert optical energy into electrical energy. In addition, multiple exciton generation (MEG) is much more efficient in QDs than bulk semiconductors and provides a promising strategy for overcoming the Shockley–Queisser (SQ) limit in traditional single-junction solar cells. Thus far, solution-processed QD solar cells have achieved a record power conversion efficiency (PCE) of $\sim 16.6\%$,¹ an impressive improvement since their introduction in 2010 with $\sim 3\%$ PCE. However, the ultimate promise of a QD based solar cell is the higher overall conversion efficiency that can be achieved via solar cells utilizing the MEG process.²

The strong light absorptivity also enables QDs to be an effective sensitizer coupled with organic chromophores. The effective electronic coupling between QDs and the organic chromophores can promote efficient spin triplet energy transfer across the QD/organic interface, subsequently the energy can be up- or down- converted to other more useful forms of photon energy through triplet-triplet annihilation or singlet fission, respectively. Recently, quantum cutting, another strategy to down-convert one high-energy photon to multiple lower-energy photons, was found to be very efficient in lanthanide doped QDs.^{3,4} In addition, the strong quantum confinement effect increases the carrier density near the QD surface, which can be exploited for interfacial charge/energy transfer between QDs and nearby molecular acceptors. Therefore, with careful design, QD-based systems can be used to convert optical energy into chemical energy that can be stored in useful chemical bonds. Additionally, when a photocatalytic reaction involves the sensitization of a spin-triplet state of the organic substrates, such as in molecular ruthenium- or iridium-based photocatalytic systems, the ill-defined spin character that exists in many QDs can reduce the energy loss from intersystem crossing between the spin-singlet and spin-triplet manifolds, thereby enhancing the energy efficiency of such photocatalytic reactions. For these reasons, QDs display tremendous potential in photocatalytic reactions. To date, QDs have been employed as efficient and robust photocatalysts for hydrogen evolution,⁵ CO₂/N₂ reduction and a variety of organic transformations⁶ including α -alkylation,⁷ β -alkylation,⁸ β -aminoalkylation,⁸ and homo- and hetero-intermolecular [2+2] cycloadditions.⁹

Here we summarize recent advances in the use and exploration of QDs for manipulating and directing the flow of optical energy (Figure 1). In particular, we highlight progress of photon conversion to electrons (*i.e.* solar cells), to other forms of photons (*i.e.* photon up-/down-conversion), and to chemical bonds (*i.e.* photocatalysis) using QDs. The advantages of using QDs

in manipulating the flow of energy over molecular chromophores are discussed, and we provide an outlook for future directions.

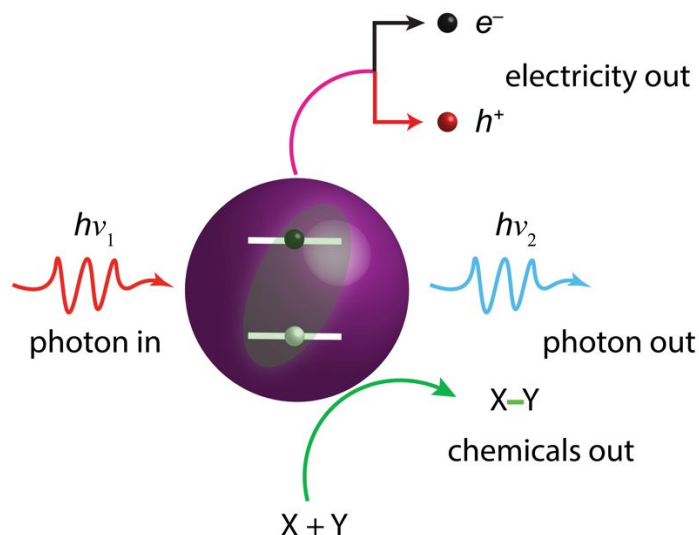


Figure 1. Manipulating flow of energy using quantum dots discussed in this review: photons \rightarrow electricity, photons \rightarrow photons, and photons \rightarrow chemical bonds.

2. Optical Energy to Electricity

2.1. Multiple Exciton Generation (MEG)

In the search for the next generation of photovoltaic (PV) absorbers, emphasis should be given to systems that have the ability to generate higher efficiencies than current single-junction technologies. In 1961, Shockley and Queisser (SQ) determined that the limiting power conversion efficiency (PCE), of a single-junction solar cell operating at AM1.5G solar flux is 33%.¹⁰ All current day single junction solar cells are effectively constrained to the SQ limit and are, thus, asymptotically approaching this limit. Generating multiple electron-hole pairs per absorbed high energy photon is a way to decrease thermalization losses and surpass the SQ limit.¹¹⁻¹⁴ Semiconductor QDs undergo multiple exciton generation (MEG) with efficiencies (defined in terms of energy conversion) greater than their bulk counterparts and thus have great potential to serve as the next generation of PV absorbers.

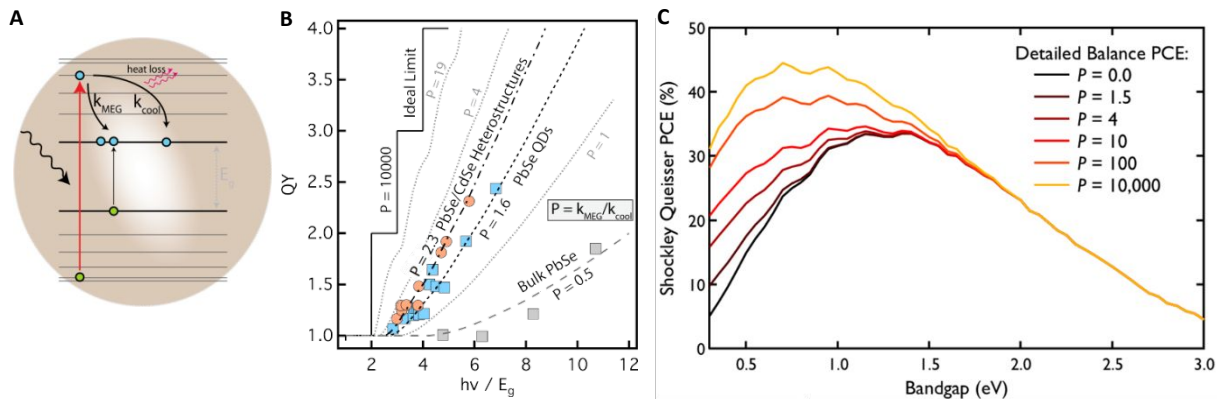


Figure 2. (A) Multiple exciton generation (MEG) occurs when a high energy photon creates a hot electron-hole pair that relaxes to the bandedge by producing another electron-hole pair. The efficiency of the process is a competition between MEG and carrier cooling via other mechanisms. (B) MEG characteristics for PbSe (bulk, grey squares), QDs (blue squares), and heterostructures (orange circles). Dashed grey lines are calculations for different values of P . (C) The theoretical limiting PCE of MEG-PV at various values of P , where $P=0$ is an absorber showing no MEG and $P=10,000$ has ideal MEG characteristics. Reprinted with permission from ref.15, Copyright 2013 American Chemical Society and ref. 16, Copyright 2016 IOP Publishing.

In an ideal MEG absorber, N excitons are created for every photon with energy $h\nu = N^*E_g$ absorbed, and the quantum yield (QY) as a function of photon energy will resemble a staircase function (Figure 2B, black trace).¹⁷ To achieve the ideal MEG characteristics, the rate of MEG (k_{MEG}) must be faster than carrier thermalization rate, or the cooling rate (k_{cool}). The phenological ratio, $P = k_{MEG}/k_{cool}$, can be used to parametrize the MEG characteristics. When $P > 10,000$ (*i.e.* when the MEG rate is 10,000x greater than the cooling rate) near ideal MEG characteristics can be reached. When $P < 10,000$, then non-ideal conditions apply. The limiting efficiency of PV cells with a single-junction MEG absorber operating at AM1.5G solar flux can be calculated using the detailed balance thermodynamic approach and is 45% (Figure 2C, yellow-trace) for the ideal MEG characteristics. The maximum efficiency is lower when MEG is not ideal.¹⁵ The optimal band gap for the maximum limiting PCE for a MEG-PV cell is 0.7 eV, compared to 1.3 eV at the SQ limit.¹³ The MEG-PV concept has a stronger dependence on solar concentration compared to non-MEG cells. Hanna *et al.* calculated that at 100x concentration the maximum PCE increases to $\sim 60\%$, whereas the limiting PCE of a bulk absorber (no MEG) at 100x is only $\sim 38\%$.¹⁴ To enhance MEG there are two strategies, (1) increase the MEG process, and/or (2) decrease the cooling channels that compete with MEG. QDs offer design parameters to impact both the MEG process via increased carrier-carrier interactions and increased density of final states and reduce carrier-phonon interactions leading to slower cooling. Nanocrystal shape (1, 2, and 3-dimensional confinement), composition, and structure (core/shell heterostructures, ligand composition, Janus-heterostructures, *etc.*) are all design parameters that can be explored for improving MEG.

2.1.1 Multiple Exciton Generation (MEG) in QDs

Two important experimental characteristics of MEG are the threshold photon energy, $h\nu_{th}$, at which the QY begins to exceed unity, and the electron-hole pair creation energy, ε_{eh} , which is the amount of excess photon energy (energy above $h\nu_{th}$) needed to produce an additional e-h pair. An energy efficiency for MEG can be defined as $\eta_{MEG} = \varepsilon_{eh}/E_g$. Lead chalcogenide QDs (PbE; E=S, Se, or Te) have been the most widely studied systems for MEG isolated in solution^{12,18-25} or in QD films with varying degrees of electronic coupling.²⁶⁻³¹ Most studies find $h\nu_{th}$ is $\sim 2.6-3E_g$, and η_{MEG} of 0.4, a significant enhancement over bulk PbSe which exhibits $h\nu_{th}$ of $\sim 6-7E_g$ (Figure 2B). In fact, $h\nu_{th}$ in bulk PbSe is limited by momentum conservation to $4E_g$ and the QD systems are already below that limit. The primary limitations for PbE QDs relates to their strong electron-phonon coupling and optical selection rules. For example, both Stewart *et al.*²² and Midgett *et al.*²⁴ found that although PbS and PbSe QDs have nearly identical k_{MEG} , the MEG yields in PbS QDs are lower than PbSe QDs due to stronger electron-phonon coupling and larger phonon energies in PbS. Since the effective masses of electrons and holes are approximately equal, optical selection rules suggest that to have $1E_g$ excess energy in either the conduction or valence bands, the absorbed photon should be $\sim 3E_g$. For these reasons Pb chalcogenide appear to be limited in their MEG efficiency.

Other QD systems that have been studied for MEG include Si,³²⁻³⁴ Ge,³⁵ InAs,^{36,37} InP,³⁸ Ag₂S,³⁹ CdTe,⁴⁰ CuInSe₂⁴¹ and Pb-halide perovskite QDs.^{42,43} The strategies for exploring these different systems relate to overcoming one of the limitations of the PbS and PbSe QDs. For Si, the advantage is that the carrier cooling could be slowed due to the interplay of carriers within the different valleys of the conduction band. Excitation into the direct Γ -valley (high-energy photon) should result in slowed cooling of electrons into the indirect valley. Such a strategy was initially pursued in SiGe bulk alloys by Queisser and co-workers.⁴⁴ Alloying Si with Ge moves the direct/indirect offset closer to the $1E_g$ excess energy ideal limit. InAs and InSb QDs have the potential to increase the MEG efficiency over PbS and PbSe because of the large effective mass of the hole, such that to produce $1E_g$ excess energy in the conduction band requires close to a $2E_g$ photon. Furthermore, CuInS₂ and Ag₂S QDs break the symmetry between the conduction and valence band resulting in a lower $h\nu_{th}$ and do not possess toxic heavy-metals.

Adding shape complexity beyond spherical QD systems allows for enhancing the rate of MEG. The Coulomb energy is greater in 2- and 1-dimensions compared to the 3D interaction in QDs. A few researchers have explored either 1-dimensional nanostructures, or quantum rods (QRs)⁴⁵⁻⁴⁷ or 2-dimensional nanostructures or quantum platelets.⁴⁸ Some enhancement in the MEG process is observed in these structures, but more studies are needed in order to better understand the various factors that govern MEG.

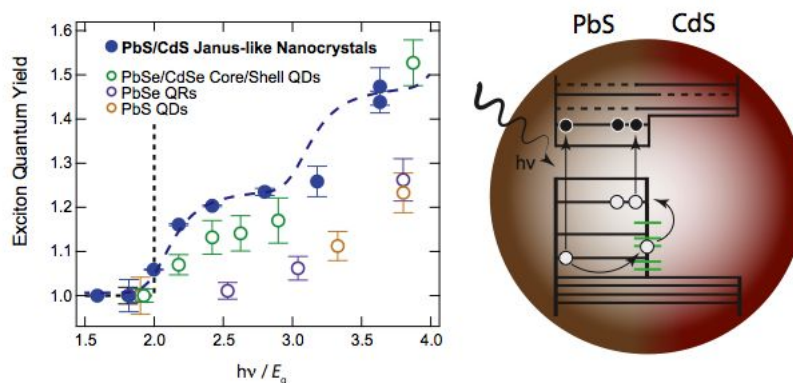


Figure 3. MEG results for Janus and core/shell heterostructures, nanorods, and quantum dots. The blue circles are for the Janus heterostructures, green circles are for core/shell structures and the purple and yellow circles are the PbS and PbSe single component spherical QDs. Left panel shows the interplay of the photoexcited carriers within the PbS component with interface states, which mediate the MEG process. Reprinted with permission from ref. 49. Copyright 2018 American Chemical Society.

2.1.2 Nanoheterostructures for MEG

A promising way to reduce the phonon-carrier interactions and increase Coulomb coupling is to design structures with asymmetry. For example, fused PbS|CdS structures termed “Janus”⁴⁹ core particles and PbSe|CdSe core-shell particles⁵⁰ are systems that have demonstrated slowed cooling and enhanced rates of MEG. The PbSe|CdSe core-shell QDs have a threshold of $2.2E_g$, a result attributed to the asymmetry introduced by the heterostructure design. PbS|CdS Janus core QDs (Figure 3) show a $\sim 2E_g$ MEG threshold. The enhanced MEG results from rapid hole trapping at the PbS-CdS interface.⁴⁹ Therefore, the heterostructure design mostly serves the purpose of providing the interfacial states that effectively slow carrier relaxation. These two studies demonstrate proof that MEG can be enhanced by carefully designing nanostructures that have features to slow down the loss pathways of hot carriers, making MEG competitive with cooling. These metal chalcogenide heterostructures are a step forward to nanostructures with ideal MEG characteristics that can then be incorporated into QD PV architectures.

2.1.3 MEG in QD Solar Cells

There are several examples of MEG measured in the photocurrent of devices incorporating QDs. Multiple carrier collection per photon was observed in the biased internal quantum efficiency (IQE) of a PbS QD photo-diode structure.⁵¹ A tandem polymer/PbSe QD device also showed evidence of MEG within the PbSe QD layer.⁵² Sambur *et al.* found by sensitizing atomically flat single-crystals with a monolayer of PbS QDs, precise IQE measurements could be performed, and they found that the IQE exceeded 100% at $\sim 2.9E_g$ of the PbS QDs.⁵³ Semonin *et al.* demonstrated a PbSe QD PV device with $>100\%$ external quantum efficiency (EQE) (Figure 4).⁵⁴ They reported an EQE of 114% with an IQE of 130%. In good agreement with the results of Sambur *et al.*, as well as solution phase ultrafast spectroscopy measurements, the threshold photon energy, $h\nu_{th}$, was

measured to be $\sim 2.8E_g$. MEG has also been detected in the EQE of solar cells made from PbSe nanorods⁵⁵ and PbTe QDs.⁵⁶ These results indicate that the limitation in exploiting MEG for solar cells resides in finding ways to increase MEG in isolated QDs and then incorporating those structures into device architectures that can harvest those carriers.

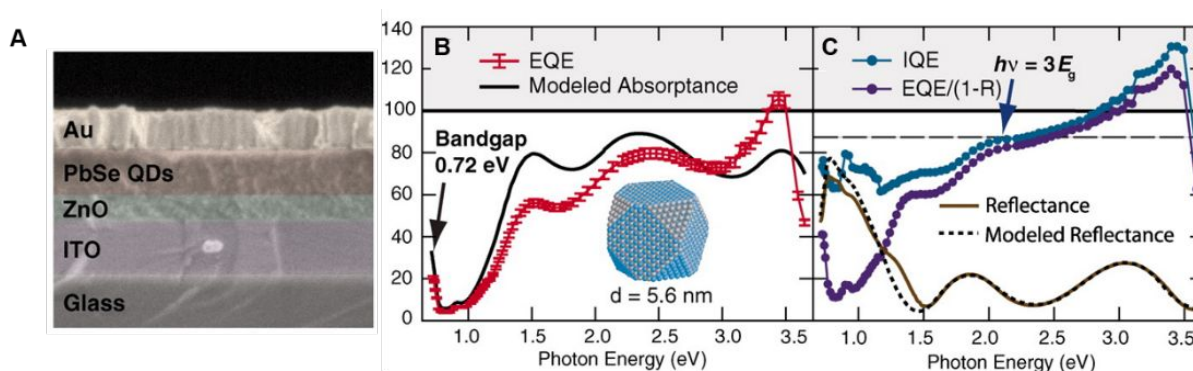


Figure 4. (A) Device configuration of the p - n QDPV device with MEG, and the associated (B) EQE and (C) IQE spectra of the 5.6 nm PbSe QDs showing $>100\%$ quantum efficiency. Reprinted from Ref. 54. Copyright 2011, American Association for the Advancement of Science.

2.1.3 Need for More Robust and Rapid MEG Screening

To further understand the QD design strategies needed to push the MEG to the ultimate limit and thereby identify new systems with enhanced MEG characteristics there is a need for new faster and more robust means of testing/screening for MEG, as well as, theory to predict promising systems for exploration. The typical approach to measure MEG yields of isolated QDs in colloidal solutions has traditionally been ultrafast transient absorption (TA) spectroscopy or in more limited cases time-resolved photoluminescence (TRPL).^{12,57-60} When using these techniques to search for new QD systems with enhanced MEG yields it is important to understand that complications can arise if proper care is not taken when making the measurements. In these ultrafast spectroscopic measurements, the evidence that multiple excitons are produced per absorbed photon is the appearance of a fast multiexciton decay component in the transient dynamics when the sample is photoexcited above the energy conservation threshold ($h\nu > 2E_g$), but in the limit where every photoexcited QDs has only absorbed at most one photon. Careful measurements of the multiexciton decay should be made with photon energies that are less than the energy conservation threshold, but with a higher photon fluences (*i.e.*, conditions where some QDs have absorbed two photons). If the dynamics in the two experiments match, then one can infer that MEG has occurred for the higher photon energies. The number of e - h pairs created per absorbed photon (the exciton quantum yield, QY) can be obtained by analyzing the amplitude of the single- and multi-exciton components (for this analysis, single exciton lifetimes must be much greater than multi-exciton lifetimes). Initially, there was much debate over TA measurements because there was a large spread in reported QYs.^{12,57,60-64} After much work, researchers concluded that some of the

discrepancies and variations could be attributed to photo-charging that can occur when using high energy photons and pulsed laser experiments.^{17,65-67} Photo-charging occurs via the creation of photo-ionized, charged QDs and whose charge state can live for a long time (in some case seconds). Using lower fluences and rapidly flowing or stirring the solutions during the measurements can minimize or eliminate such photo-charging effects. We refer interested readers to several reviews of the MEG measurements that detail these complications.^{58,59,63,65,66} Photocurrent measurements are not impacted in the same way and would result in a decrease in the internal quantum efficiency (IQE) (for photocurrent generation). Thus, the concurrence of photocurrent and TA measurements give assurance that these photo-charging effects are not impacting the results.

In addition, the transient spectroscopic measurements are laborious and time consuming. Solar cell architectures where current is measured are preferable. However, developing a QD solar cell from QD systems can also be time consuming and thus knowing whether high MEG yields are possible prior to undertaking such an endeavor is necessary. We recommend that the community should develop new device current-based approaches for measuring enhanced light-to-current yields, but which are less complex than a solar cell. For solar cells, the basic strategy is to sandwich a QD-layer between an *n*-type window layer, which accepts electrons while blocking holes, and a metal electrode that accepts holes. Light is absorbed in the QDs and excitons separate to form free electrons and holes. Critical issues that need to be addressed are robustness of QD-layer formation and optimization of the front and back interfaces. Adapting such architectures for fast and reliable MEG measurements could greatly benefit the search for systems with enhanced MEG characteristics.

2.2. QD Solar Cells

Ultimately, in order to take advantage of MEG in QDs, solar cells made from QDs need to be developed that have PCEs on-par with solar cells made from bulk and thin-film systems. Beyond MEG, QDs make interesting PV systems due to their tunable parameters, such as absorption edge, band positions, doping, different processing conditions, and ease of preparation. The early realizations of QD solar cells began with the use of QDs as an optical sensitizer which injects the photogenerated electron into mesoporous TiO₂ (QD-sensitized solar cell).⁶⁸⁻⁷⁰ Another design is a bulk heterojunction with QDs embedded into a conductive polymer matrix.⁷¹⁻⁷⁴ The early designs were followed by the use of QDs as both the absorber and charge transport layer, such as Schottky⁷⁵⁻⁷⁷ and *p-n* junction architectures.⁷⁸ The main challenge in quantum dot photovoltaics (QDPVs) is adapting new structures which can transport photogenerated carriers relatively long distances despite the number of “interfaces” encountered in a QD-based network. So far lower charge carrier mobilities and diffusion lengths are reported for QDs arrays than most bulk systems (other than organic systems). However, by tuning the various physical and chemical parameters, PCEs are improving. Synthetic methods for controlling the optoelectronic properties provide a means of generating high efficiency QDPVs. PCEs of up to 13.1%⁷⁹ have been achieved in metal chalcogenide QDPVs and up to 16.6%^{80,81} in perovskite QDPVs. We expect that this progress

will continue as new researchers enter this area with novel approaches. It is important for researchers to utilize the unique aspects of QDs when designing new architectures rather than simply considering them as a different thin-film system. For example, Bawendi and co-workers utilized the fact that different band-edge positions can be produced depending on the surface conditions of the QDs (see discussion below).⁸² They used this knowledge to build a charge separating interface *within* the QD arrays. Similarly, Luther and co-workers employed the ability to process the QDs sequentially and the added phase stability of perovskite QDs to build a similar internal charge-separating interface.⁸⁰

An important parameter in designing QDPV architectures are the QD surface ligands. Metal chalcogenide QDs are most often synthesized with long-chain alkyl groups, such as oleic acid (OA), oleylamine, and trioctylphosphine. In colloidal particles, the alkyl ligands can help control the growth, and are responsible for solution stability and passivation of surface states for high PL quantum yields. Due to the insulating nature of the native aliphatic ligands, QDs used for PV systems typically have their ligands exchanged with either shorter organic ligands, inorganic complexes, or single-atom ionic species.⁸³ The short ligands produce a variety of effects in QD solids and can offer many ways to tune their emergent properties. Through ligand exchange, the inter-particle distance, mobility, majority carrier type,⁸⁴ band positions,⁸⁵ trap density,⁸⁶ and optical density⁸⁷⁻⁸⁹ can all be controlled. The chemical nature of the ligand can also affect the majority carrier type and Fermi level. For instance, exchanging native ligands with thiols like ethanedithiol (EDT) decreases the M:S (M = Pb or Cd) stoichiometry, producing an *p*-type film.⁹⁰ Conversely, *n*-type films can be produced by exchanging with amines, potassium,⁹¹ indium,⁹² and halides.^{84,91,93} One key breakthrough of QDPV was the introduction of dual ligand treatments. Semonin *et al.* found that a layer of EDT treated PbSe QDs followed by a layer of hydrazine treated PbSe QDs increased the V_{oc} in large diameter PbSe QD solar cells.⁹⁴ Bawendi and co-workers⁸² developed a double treatment for PbS QDs using EDT and TBAI. They found that the increased V_{oc} and increased PCE resulted from differences in the work function of the QD-films when treated individually with EDT and Tetra-*n*-butylammonium iodide (TBAI), and that combining the two treatments produces an internal charge separating junction. Nearly all high efficiency PbS QD solar cells now use a process where there are two layers of QDs with different final ligands.^{95,96,85} Recent developments are pursuing the use of shorter and more polar solution phase ligand exchanges. New polar solvents are used to support shorter polar ligands that are exchanged with the longer ligands prior to QD film formation. PbI_2 in DMF was found to remove nearly all of the as-produced organic ligands and form close packed PbS QD films with PbI_2 decorating the surfaces.^{73,97} The thickness of the absorber layer could be increased to ~ 800 nm with little degradation to the solar cell performance, nearly thick enough to absorb all of the incident solar irradiance above the QD band gap. Recent work from Sargent and co-workers has further extended the PbI_2 treatments to produce some of highest PCEs from PbS QD solar cells.⁹⁵ In addition, combining useful properties of organic layers with QD layers is being explored as a way to increase the light harvesting in QD/hybrid solar cells.⁷⁹

2.2.1 Tandem QD Solar Cells

Another means of exceeding the single-junction SQ limiting efficiency is by using a multi-junction architecture, where a cascading interconnected stack of solar cells with progressively smaller bandgaps is employed to reduce thermalization losses. This approach is common for high efficiency III-V solar cells and to date is the only current approach where a solar cell exceeds 33% power conversion efficiency under one-sun illumination. There are features of QDs that makes this approach enticing here too. Colloidal QD processing does not require lattice matching and thus could greatly simplify the manufacturing procedure. In addition, the size tunability of QDs allows for precise optimization of bandgaps for splitting the solar spectrum and provides a path for a multi-junction cell made from a single absorber material. Notably, PbS QDs can be tuned to the ideal bandgaps for a triple junction cell: 0.71 eV, 1.16 eV and 1.83 eV.⁹⁸

The design principles for constructing multijunction QD solar cells are certainly more stringent than for single junction QD devices. While the sub cell structure appears to simply connect two subcells using a recombination layer, for the performance to exceed that of a single junction cell, each subcell must be optimized to most efficiently convert the photons just above their band edge. Since the absorption coefficient is lower for photon energies just above the band edge, compared to that for higher energy photons, in practice, the absorber layer must be thicker and thus requires better charge-carrier transport properties (larger diffusion length of carriers). Another constraint is that the contact layers and recombination layer must minimize light absorption.

As a proof of concept, Choi *et al.* reported a tandem cell using an interconnecting layer of ZnO/Au/PEDOT:PSS between the 1 eV and 1.6 eV PbS QD cells.⁹⁹ The thin gold layer was found to be crucial for minimization of series resistance from the interlayer. Wang, Koleilat and colleagues reported a depleted heterojunction tandem using a graded recombination layer consisting of a stack of metal oxides with a progression of work functions.¹⁰⁰

Another approach incorporating thin film QD-layers in a tandem configuration is to deposit the QD-layer on a different PV technology, for example Si, CdTe, CIGS, *etc.*. A tandem QDPV structure was fabricated by Crisp *et al.* with CdTe/PbS QD absorbers which generated 5% PCE, with a high V_{oc} of 1.13 eV and J_{sc} of ~ 10 mA/cm².¹⁰¹ This configuration featured a PbS QD device inverted from standard design to match the polarity of the bottom CdTe cell and a ZnTe-ZnO recombination layer. In their report, the champion device was made by optimizing the thickness of the CdTe such that some of the higher energy light passed through to the PbS QD layer. The optimum thicknesses were 300 and 700 nm for the CdTe (0.98 eV) and PbS (1.1 eV), respectively.

2.2.2 Pb-Halide Perovskite QD Solar Cells

The last two highest record efficiencies on the QD track of the NREL PV efficiency chart were set by perovskite QDs of the major composition of CsPbI₃, now with a record of 16.6%.^{1,81} The generic perovskite formula is ABX₃. Figure 5A shows the cubic perovskite unit cell with the lead (B-site,

green) halide (X-site, red) octahedra sharing corners and cesium (A-site, purple) in between. The CsPbX_3 ($X=\text{Br}, \text{I}$) nanocrystals, first synthesized by Protesescu *et al.*¹⁰² have unusual defect tolerance, reflected in their bright luminescence (PLQY $\sim 100\%$), especially green, and band gaps ranging from 1.85–2.12 eV. Compared to thin film perovskite systems, perovskite QDs offer unique chemical, crystallographic and morphological turnabilities for solar cells that are unattainable by their bulk analogues. Thin film bulk perovskite solar cells, which now have demonstrated 25.2% PCE,¹ most commonly have a small organic cation in the A-site, such as methylammonium (CH_3NH_3^+) and formamidinium ($\text{CH}(\text{NH}_2)_2^+$). However, overall device stability is a significant challenge for the organic-inorganic hybrid perovskites, and the substitution of the organic cation for Cs is one way to circumnavigate this challenge. However, Cs^+ is considered too small of an A-site cation for $[\text{PbI}_6]^{4-}$ octahedra (based on Tolerance factor)¹⁰³ and thin film CsPbI_3 is only metastable in the perovskite phase at temperatures over 320 °C. This phase stability issue can be addressed by reducing the dimensions to the nanoscale, namely QDs. In the 15 nm range, CsPbI_3 QDs exhibit strong tensile surface strain which stabilizes the perovskite phase.¹⁰⁴ Swarnkar *et al.* developed the first perovskite QD solar cell based on this material and have shown reproducible J-V characteristics over several weeks (Figure 5B), thereby making them a viable PV system.¹⁰⁵

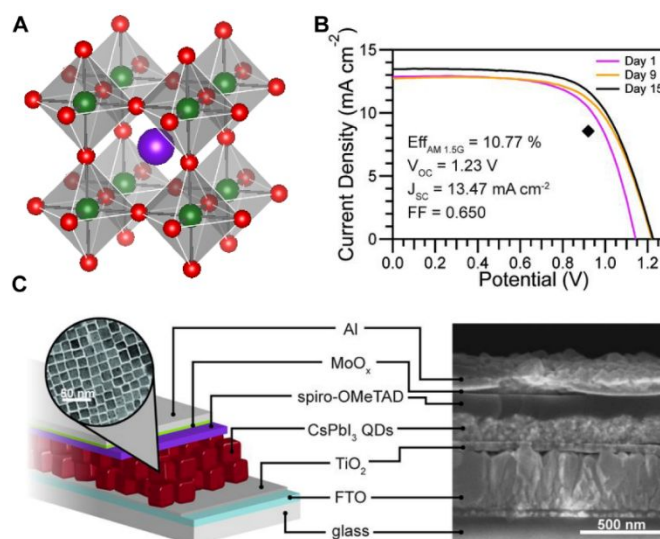


Figure 5. (A) Cubic all inorganic CsPbI_3 perovskite unit cell, (B) J-V curve for CsPbI_3 QDPV cell, and (C) the corresponding device stack of the data in (B). B and C were reprinted from ref¹⁰⁵. Copy 2016, American Association for the Advancement of Science.

The QD films are made via sequential spin coating or drop casting a solution of perovskite-QDs onto a transparent metal oxide substrate until sufficient thickness is achieved. Figure 5C shows a typical perovskite-QD device stack and micrograph cross section. Based on this design, V_{oc} of 1.23 V and J_{sc} up to $>13 \text{ mA/cm}^2$ were achieved with PCEs reaching $>10\%$.¹⁰⁵ PCE above 13% was achieved in the study by Sanehira *et al.*, where they explored the dependence of PCE on film post treatment using formamidinium iodide (FAI), methylammonium iodide (MAI), CsI, and the

bromide salts of FA^+ and MA^+ .¹⁰⁶ They found that the FAI post treatment produced the best overall PV performance (PCE of 13.4%, V_{oc} of 1.20 V, J_{sc} up to 14.37 mA/cm^2) and the highest charge-carrier mobility (0.50 cm^2/Vs) of the treatments studied. In a recent development, Zhao *et al.*⁸⁰ fabricated $\text{Cs}_x\text{FA}_{1-x}\text{PbI}_3$ QDPV devices with highly efficient charge separating heterojunctions, which was enabled by the full-range tuning of A-site cation composition in colloidal QDs, namely $\text{Cs}_x\text{FA}_{1-x}\text{PbI}_3$ QDs.¹⁰⁷ The heterojunction devices made from $\text{Cs}_x\text{FA}_{1-x}\text{PbI}_3$ QD layers of different Cs:FA ratios produced J_{sc} as high as 19.2 mA/cm^2 , V_{oc} of 1.21 V, PCE of 17.4% (in separate devices). Similarly, Wang and co-workers⁸¹ fabricated QDPVs based on $\text{Cs}_x\text{FA}_{1-x}\text{PbI}_3$ QDs, which is prepared by a ligand-assisted cation exchange reaction, and they were able to achieve a certified record PCE of 16.6% with negligible hysteresis. The QD devices were also demonstrated to exhibit significantly enhanced photostability compared to the thin-film counterparts due to suppressed phase segregation. Many perovskite QD PV devices described here show high open circuit voltage and can lend approaches to improving thin film perovskite PV.^{108,109} Clearly, the efficiencies of state-of-the-art perovskite QDPVs are approaching other solution-processable photovoltaic technologies (*e.g.* organic solar cells, thin films), while at the same time providing unique opportunities for surpassing the theoretical S-Q limits.

3. Optical Energy Interconversion

3.1 Triplet Exciton Involved Photon Up-/Down-Conversion

Exciton multiplication processes, *e.g.* photon up- or down conversion, are potential strategies to boost the solar energy conversion efficiency and surpass the Shockley-Queisser limit for single junction solar cells. Specifically, up-conversion¹¹⁰ combines multiple low-energy photons into one high-energy photon, while down-conversion¹¹¹ splits one high-energy photon into multiple low-energy photons, two promising ways to reduce transmission and thermalization losses, respectively, in solar cell architectures. In order to realize efficient up- or down-conversion, spin-triplet excitons are typically involved, as the long lifetime of triplet excitons allows for an efficient energy transfer within up-/down-conversion schemes.

3.1.1 Triplet Fusion Based Photon Up-Conversion

Triplet-fusion based photon up-conversion is capable of directly using the photons under solar flux.¹¹² This is a key advantage against lanthanide doped up-conversion systems,¹¹³ which need excitation intensity orders of magnitude higher than is available from the solar flux. As shown in Figure 6A, photon up-conversion is initiated with the excitation of a light absorber with strong absorptivity and high efficiency of intersystem crossing to yield triplet excitons. The triplet energy is then transferred to a light-emitter, namely an organic dye, which typically possess a high fluorescence quantum yield. Two emitter molecules in the triplet excited state meet, and the triplets fuse to form a higher-energy singlet (also termed ‘triplet-triplet annihilation’), followed by emission of the up-converted photon from the singlet state. Triplet-fusion based photon up-conversion can be sensitized with either an organic dye¹¹⁴ or a semiconductor QD.¹¹⁵ QYs as high

as 36% have been observed in molecular system (*i.e.* organic dyes).¹¹⁶ Semiconductor QDs serving as the light absorber for photon up-conversion schemes was first reported by Huang *et al.*¹¹⁷ in 2015 where cadmium and lead chalcogenide QDs were used to convert visible and near infrared (NIR) light respectively (Figure 6A,B). The same strategy was also reported by Wu *et al.*¹¹⁸ where PbS QDs were used as the triplet sensitizer for triplet fusion based photon up-conversion in solid films. Compared to molecular absorbers, semiconductor QDs show a broader absorption band and stronger light absorptivity. Additionally, the bandgap of the QDs can be easily tuned by composition and/or size, continuously extending from the near ultraviolet to the near infrared. The ease of QD synthesis and their higher photostability are also merits for QDs and against molecular absorbers.

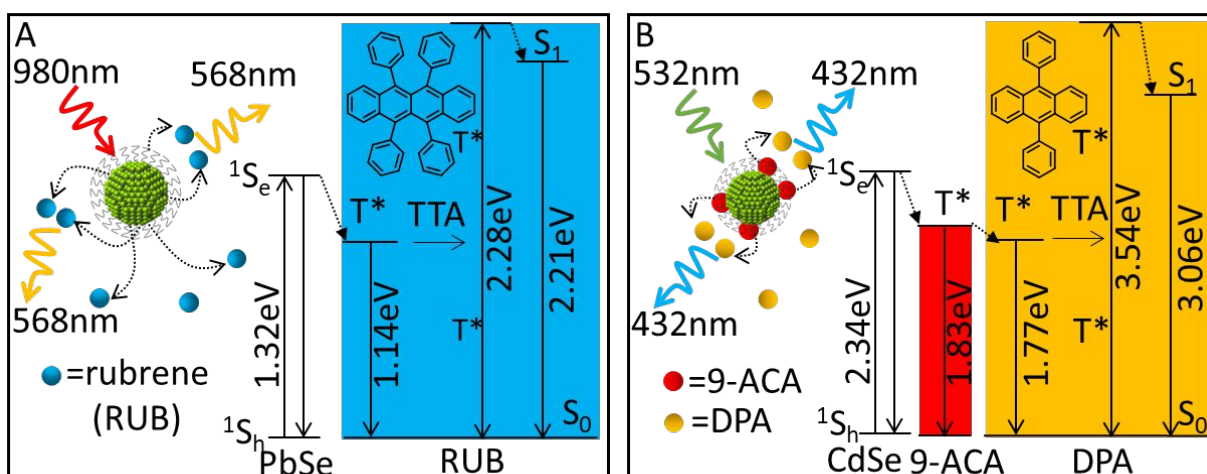


Figure 6. Illustration of quantum dot (QD) sensitized photon upconversion. (A) PbSe QD sensitized near infrared-to-visible upconversion combined with rubrene (RUB, blue dots) as the light emitter. (B) CdSe QD sensitized visible-to-near ultraviolet photon upconversion. CdSe QD are functionalized with 9-anthracenecarboxylic acid (9-ACA, red dots) which funnels the energy to the emitter 9,10-diphenylanthracene (DPA, yellow dots). Reproduced from ref ¹¹⁷. Copyright 2015 American Chemical Society.

The efficiency of triplet energy transfer Φ_{TET} is one of the limitations for efficient upconversion.¹¹⁹ Significant effort, therefore, has been expended on the optimization of Φ_{TET} by the design and modification of both the QD core and surface bound ligands. Researcher have found that functionalization of the QD with surface anchored acene ligands, with the proper triplet energy alignment, can vastly enhance the Φ_{TET} .¹¹⁷ Native ligands of as-synthesized QDs are typically long aliphatics which serve as a barrier for the triplet energy transfer from the QD to the emitter. Functionalization of the QD surface by acene ligands that are short in length and have low lying triplet energy states can funnel the triplet energy from the QD to the emitter, thereby enhancing Φ_{TET} and the resulting total up-conversion QY, Φ_{UC} (Figure 6B). Anthracene functionalized CdSe QDs yield a Φ_{UC} of 14%, compared to 0.1% with no functionalization.¹²⁰ Similarly, tetracene ligands anchored on lead chalcogenide QDs enhance the NIR-to-visible up-conversion QY by 80 times.¹²¹ As for mechanistic studies, surface anchored anthracene triplets were directly observed

in the transient absorption spectra when selectively exciting CdSe QD donors.¹²² A Dexter-type energy transfer mechanism was demonstrated by an exponential dependence of the transfer rate with QD-molecule distance.^{120,123}

Photophysical properties of the QDs play a key role in the energy transfer and Φ_{UC} .¹¹⁵ Size dependence has been observed for both CdSe QD sensitized visible up-conversion and lead chalcogenide QD sensitized NIR up-conversion.^{124,125} As a triplet energy donor, small QD sizes with higher exciton energies lead to higher Φ_{TET} and Φ_{UC} . The high Φ_{UC} with small QDs, however, is at the expense of the small anti-Stokes shifts between the absorbed and emitted photons. Therefore, proper QD size should be used to balance the QY and anti-Stokes shift to maximize the energy conversion efficiency. Due to the large surface area-to-volume ratio of the QDs, dangling bonds and other surface defects are attributed as the main reasons that limit the photoluminescence QYs or exciton lifetimes for an efficient energy/charge transfer. For up-conversion, it has been shown that the up-conversion QY positively correlate with the photoluminescence QY of QD.¹¹⁵ In light of this, inorganic shells were grown on QD cores to eliminate surface traps and improve the PL QD.¹²⁶⁻¹²⁸ Φ_{UC} was enhanced by 1.6 times by growing a sub-monolayer CdS shell on PbS core.¹²⁹ This enhancement is due to the suppression of a surface trap induced hole transfer from QDs to the molecules, observed in transient absorption spectra. It is worth noting that trap states with proper energy positions can also facilitate the triplet transfer from QDs to molecules. Bender *et al.*¹³⁰ showed that instead of direct triplet transfer from PbS QDs, the triplet state of surface bound TIPS-pentacene is produced from an intermediate state which is assigned to surface trapped charge carriers. Han *et al.*¹³¹ reported that CuInS₂ QDs produce long lived self-trapped excitons which are transferred to molecular acceptors with an efficiency of 92.3%. With trap assisted triplet energy transfer, an up-conversion QY of 18.6% was realized, which is the current record for QD sensitized photon up-conversion.

Other than II-VI and IV-VI QDs, perovskite QDs are also an alternative for triplet sensitization and up-conversion. Kimizuka and co-workers¹³² reported the first use of CsPbX₃ perovskite QDs to sensitize visible up-conversion with the up-conversion QY of 1.3%. Wu and co-workers¹³³ later revealed that the low triplet energy transfer efficiency is due to weak quantum confinement effects in larger sizes of CsPbBr₃ QDs. In contrast, smaller sized CsPbBr₃ QDs with concomitant stronger quantum confinement possess higher carrier probability densities at their surfaces, which results in stronger electronic coupling with the attached acceptors, thereby, promoting the triplet energy transfer. With this in mind, they demonstrated that the triplet energy transfer efficiency can be enhanced to ~99% in 3.5 nm strongly confined CsPbBr₃ QDs using 1-pyrenecarboxylic acid as the triplet acceptor. They further reported¹³⁴ that CsPbBr₃ QDs with surface anchored 1-naphthalene carboxylic acid, and 2,5-diphenyloxazole as the emitter, yields visible-to-ultraviolet up-conversion with 10.2% QY.

3.1.2 Singlet Fission Based Photon Down Conversion

Singlet fission has been widely studied with organic dyes.¹¹¹ As the reverse of triplet fusion (discussed above), singlet fission describes the generation of two triplet excitons from one singlet exciton. Specifically, an organic chromophore in the singlet excited state shares its energy with a ground-state chromophore that is in close proximity, yielding two triplets. This spin-allowed process can be very efficient as it typically occurs in a femto- or pico-second time scale and out-competes other exciton decay processes. In solar energy conversion, by splitting one high-energy excited state to two low energy-excited states (analogous to the MEG process described above), singlet fission is able to harvest energy that would otherwise be lost to thermalization and can thereby enhance the overall photocurrent and power conversion efficiency. For example, with the quantitative conversion of one singlet pentacene to two triplets, Congreve *et al.*¹³⁵ obtained 109% EQE in organic based photovoltaic cells.

In addition to charge separation and the subsequent collection of those charges, the triplet excitons can also be harvested via luminescence. “Singlet fission photon multiplier” takes use of the luminescence from the singlet fission generated triplet excitons for photovoltaics cells.¹³⁶ However, the emission of triplets in non-metallic organic systems is spin forbidden. One strategy to overcome this limitation is by using organic-metal complexes with high intersystem crossing efficiency, which has proven successful in organic light-emitting devices.¹³⁷ However, in the near-infrared regime, the performance of organic dyes is poor because of their strong internal conversion.^{138,139} In view of this, semiconductor QDs could potentially be an excellent triplet harvester. This is because the lowest triplet state of the QDs could be emissive by overcoming the small exchange energy (~ 12.5 meV)¹⁴⁰ and fast conversion to the emissive singlet state at room temperature. This allows the potential use of QDs as an excellent near infrared emitter.

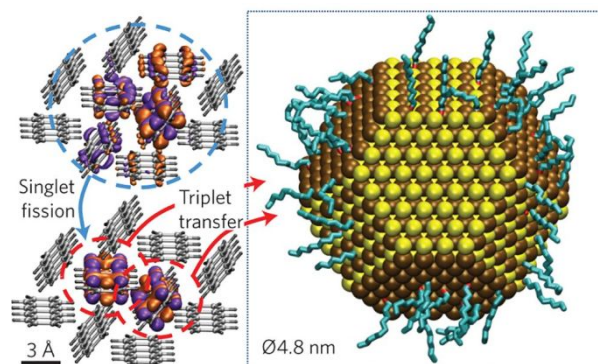


Figure 7. Singlet fission of tetracene is followed by triplet energy transfer to PbS QDs, which doubles photoluminescence QYs of PbS QDs. Reproduced from ref ¹⁴¹. Copyright 2014 Nature Publishing Group.

Triplet energy transfer between molecules and semiconductor QDs was not well recognized until two back-to-back publications from Rao's and Baldo's groups in 2014. With transient spectroscopy, Rao and colleagues¹⁴² observed triplet energy transfer from pentacene to PbSe QDs after singlet fission within the pentacene molecules. This triplet energy transfer is a resonant transfer based on a QD size dependent study. Similarly, Baldo and co-workers¹⁴¹ reported the

singlet fission of tetracene and the subsequent transport of the generated triplet excitons to PbS QDs (Figure 7). This was proven by the enhanced photoluminescence of the PbS QDs. Calculations based on the enhanced photoluminescence shows that the efficiency of tetracene singlet fission and triplet transfer to PbS QDs are both near unity.

Following these pioneering reports, different molecule-QD hybrid systems have been designed for efficient singlet fission. Nathaniel *et al.*¹⁴³ reported a doubled photoluminescence QY of PbS QDs by anchoring TIPS-tetracene ligands on the QD surfaces. In that work, TIPS-tetracene ligands are directly photoexcited and undergo singlet fission to yield two triplets, which are sequentially transferred to the PbS QDs, followed by light emission from the PbS QDs. Considering the doubled photoluminescence QYs, the efficiency of TIPS-tetracene singlet fission, as well as, the triplet energy transfer to PbS QDs should be near unity. Similar to the up-conversion analogy, Allardice *et al.*¹⁴⁴ designed a three-component singlet system including PbS QDs, surface anchored and free TIPS-tetracene. In this system, over 95% of the incident light is absorbed by the free TIPS-tetracene to initiate singlet fission (135% efficiency). The generated triplet excitons can be quantitatively (95%) harvested with a low concentration of QDs.

In addition to the lead chalcogenide QDs, other systems can also be used as triplet acceptors after singlet fission. Baldo and co-workers incorporated tetracene as a single fission layer in Si solar cells.¹⁴⁵ The singlet fission generated triplet excitons were transferred to an underlying Si solar cells efficiently, the triplet energy transfer was assisted by an electric-field-effect passivation. The combined yield of singlet fission and triplet transfer reached 133%. Other than the light emitter, QDs can also work as a light absorber to sensitize singlet fission. Compared to the singlet fission of organic dyes, QD sensitizers possess stronger and broader absorption bands. Beard and co-workers reported that CsPbBr₃ perovskite QDs can transfer energy to the singlet state (79% efficiency) of surface bound TIPS-pentacene which then undergoes singlet fission (145% efficiency), generating an overall yield of 113% triplets.¹⁴⁶ The singlet energy transfer is mediated through a Dexter-like electron exchange mechanism, instead of a Förster mechanism, at the CsPbBr₃/pentacene interface. Excited pentacene singlets can then undergo efficient singlet fission on the QD surface due to the sufficient intermolecular coupling provided by dense surface binding. Compared to commonly observed triplet energy transfer at the QD-acene interface, this system provides a new strategy to produce molecular triplets with a 200% quantum yield using QDs as the sensitizer.

3.2 Quantum Cutting in Lanthanide Doped Perovskite QDs

Another strategy that can down-convert one high-energy photon to multiple low-energy photons is quantum cutting (QC). QC was first observed in lanthanide elements.¹⁴⁷ Lanthanide doped nanoparticles can up-convert photons and potentially be used in biological imaging.¹¹³ QC is effectively the reverse process of up-conversion and is analogous to both the singlet fission occurring for molecular systems and MEG that occurs in QDs. In QC, one ultraviolet photon can be split into two low-energy photons with a quantum yield of over 100%.¹⁴⁸⁻¹⁵⁰ Both up-conversion

and QC in lanthanides are based on their abundant f electron configurations. Mechanisms of QC are presented in Figure 8. QC can be realized with a single luminescence center (Figure 8A). In this strategy, lanthanides are photoexcited to a high energy electronic state, followed by subsequent decay to the lower electronic state and finally to the ground state, with the emission of two or more photons. Alternatively, QC can be realized with multiple luminescence centers with cross-relaxation energy transfer involved between luminescence centers, as shown in Figure 8B-D.

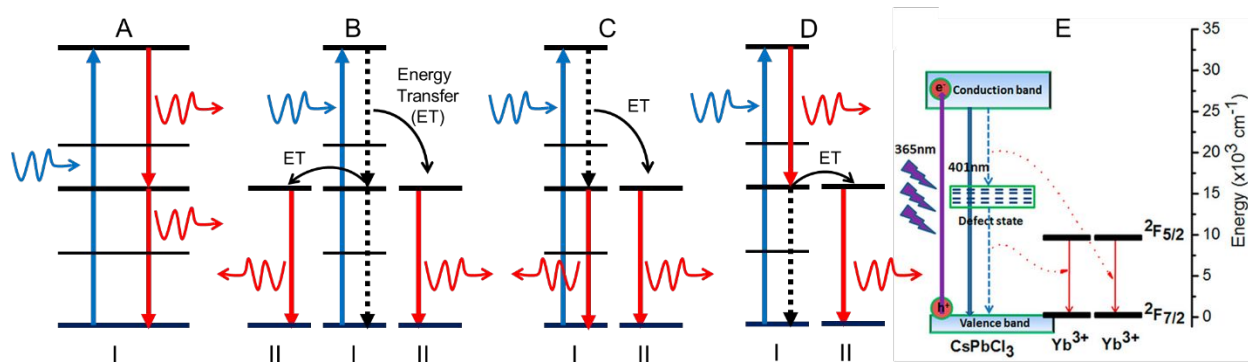


Figure 8. Four strategies of quantum cutting of lanthanide ions involving single ion (A) or multiple ion centers (B-D). (E) Quantum cutting of Yb³⁺ ion doped CsPbCl₃ perovskite quantum dots. A-D were redrawn from ref ¹⁴⁶ and E was reproduced from 3. Copyright 1999 American Association for the Advancement of Science, and 2017 American Chemical Society.

Highly efficient QC systems using lanthanides suffer from low absorption cross section, and low lanthanide concentrations are needed to avoid cross-relaxation. This problem is recently circumvented by using a new host material, namely perovskite QDs. Pan *et al.*³ developed the synthesis of a series of lanthanide-doped perovskite QDs and they observed a photoluminescence QY of 143% for Yb³⁺ doped CsPbCl₃ QDs. As shown in Figure 8E, this unexpectedly high QY is explained with the QC mechanism: the photoexcited CsPbCl₃ exciton decays to a defect state and then to the ground state, concomitant with the sequential energy transfer to two Yb³⁺ ions which subsequently emit two NIR photons. Among a series of dopants, only Yb³⁺ doping results in a photoluminescence QY over 100% because the exciton energy of CsPbCl₃ QDs perfectly matches twice the energy of Yb³⁺ 2F_{5/2}-2F_{7/2} transition. This is the first example of QC sensitized by semiconductor QDs. Following this work, a series of detailed studies were developed to understand the dopant effect and optimize the QC efficiency. Milstein *et al.*⁴ improved the near-infrared photoluminescence QY to 170% with Yb³⁺ doped CsPbCl₃ QDs. With transient absorption spectroscopy, they showed that the energy transfer from photoexcited QDs to Yb³⁺ occurs within the picosecond time scale, and the transfer is efficient at all temperatures from 5 K to room temperature.

Novel synthetic methods are also developed for Yb³⁺ doped perovskite QC systems. Traditional hot-injection methods with lanthanide chloride, lead chloride and cesium oleate are limited due to the poor solubility of the precursor, especially lanthanide chloride for samples with high lanthanide doping levels. Milstein *et al.*⁴ solved this problem by using more soluble acetate precursors that

yields Yb^{3+} doping levels of up to 7.4%. With a Cl-to-Br anion exchange reaction, Milstein *et al.*¹⁵¹ reported the synthesis of Yb^{3+} doped $\text{CsPb}(\text{Cl}_{1-x}\text{Br}_x)_3$ QDs. By controlling the degree of anion exchange with trimethylsilyl halides (TMS-X), the bandgap of the QDs were continuously tuned from 3.06 eV to 2.53 eV, while the photoluminescence QY remains the same (above 100%).

As with the photovoltaic devices, both theoretical studies and experimental results point towards the benefits of the incorporation of QC materials. Crane *et al.*¹⁵² developed a model to pair a Yb^{3+} : $\text{CsPb}(\text{Cl}_{1-x}\text{Br}_x)_3$ QC layer with different existing single junction solar cells, and silicon heterojunction solar cells showed significant performance gain, with the predicted power conversion efficiency of 32%. Cohen *et al.*¹⁵³ modeled the performance of a 1D and 2D luminescent solar concentrator incorporated with Yb^{3+} : $\text{CsPb}(\text{Cl}_{1-x}\text{Br}_x)_3$ QC QDs, and proposed a monolithic bilayer luminescent solar concentrator device with the QC layer, showing 19% enhancement of the flux gain compared with the optimized CuInS_2 luminescent solar concentrator. Experimentally, Zhou *et al.*¹⁵⁴ reported that by using Yb^{3+} , Ce^{3+} co-doped $\text{CsPbCl}_{1.5}\text{Br}_{1.5}$ QD as the QC layer, the PCE of commercial silicon solar cells can be noticeably enhanced from 18.1% to 21.5%. This work demonstrates the values and potential commercialization incorporating QC with existing solar cell technologies.

4. Optical Energy to Chemical Bonds

Upon photoexcitation, QDs can also store optical energy in chemical bonds through photocatalytic reactions. Compared to molecular chromophores, QDs display several superior properties for photocatalytic reactions. (1) QDs intrinsically possess higher absorption coefficients, which lead to less catalytic loading per reaction. (2) The quantum confinement effect provides additional parameter space to tune their absorption spectra, ranging from UV-Vis to NIR, and to modulate the electronic coupling between QDs and the molecular substrates by tuning the carrier probability density at the surface as well as a tuning of the bandedge positions. The controllable electronic coupling can mediate charge or energy transfer between QDs and molecular substrates, activating molecules, which are subsequently transformed to products through breaking or forming chemical bonds. (3) QDs can absorb multiple photons and generate multiple excitons or reducing/oxidizing equivalents per QD without decomposition or changes to the QD absorption profile. In contrast, molecular chromophores typically do not absorb multiple photons prior to relaxation and thus cannot build-up multiple reducing/oxidizing equivalents per cycle. If the generated multiple excitons per QDs per absorbed photon can be effectively converted to chemical bonds, the resulting quantum efficiency can exceed 100% in a photocatalytic reaction.

4.1 Hydrogen Evolution

Hydrogen is considered as the fuel of the future because of its high specific enthalpy and environmental compatibility upon combustion. Producing hydrogen from a photocatalytic reaction offers a promising approach to build the hydrogen economy. Although QDs are an excellent solar absorber, the photocatalytic hydrogen evolution quantum efficiency using QDs as the sole

photocatalyst is limited due to fast recombination of photoinduced charge carriers and the photocorrosion of QDs after redox chemistry. Therefore, the biggest challenge is to create an artificial system that generates long-lived charge separated states to drive the subsequent redox chemistry. As shown in Figure 9, one strategy is to couple QDs with a hydrogen evolution cocatalyst, including precious metals, molecular compounds, and hydrogenase, which can promote long-lived charge separation and also serve as the active site for hydrogen evolution.¹⁵⁵ Another strategy is to increase the physical distance between photogenerated carriers by the use of other nanostructures, such as 1D nanorods, and to decrease the wavefunction overlap between electrons and holes with the use of heterostructures, such as core/shell structures. In these systems, the QDs work as a photosensitizer to capture the photon energy, while the cocatalyst is the actual photocatalytic center. Another important strategy is to separate electrons and holes by integrating the QDs into a photoelectrochemical cell, thereby separating the reductive process from oxidative process.

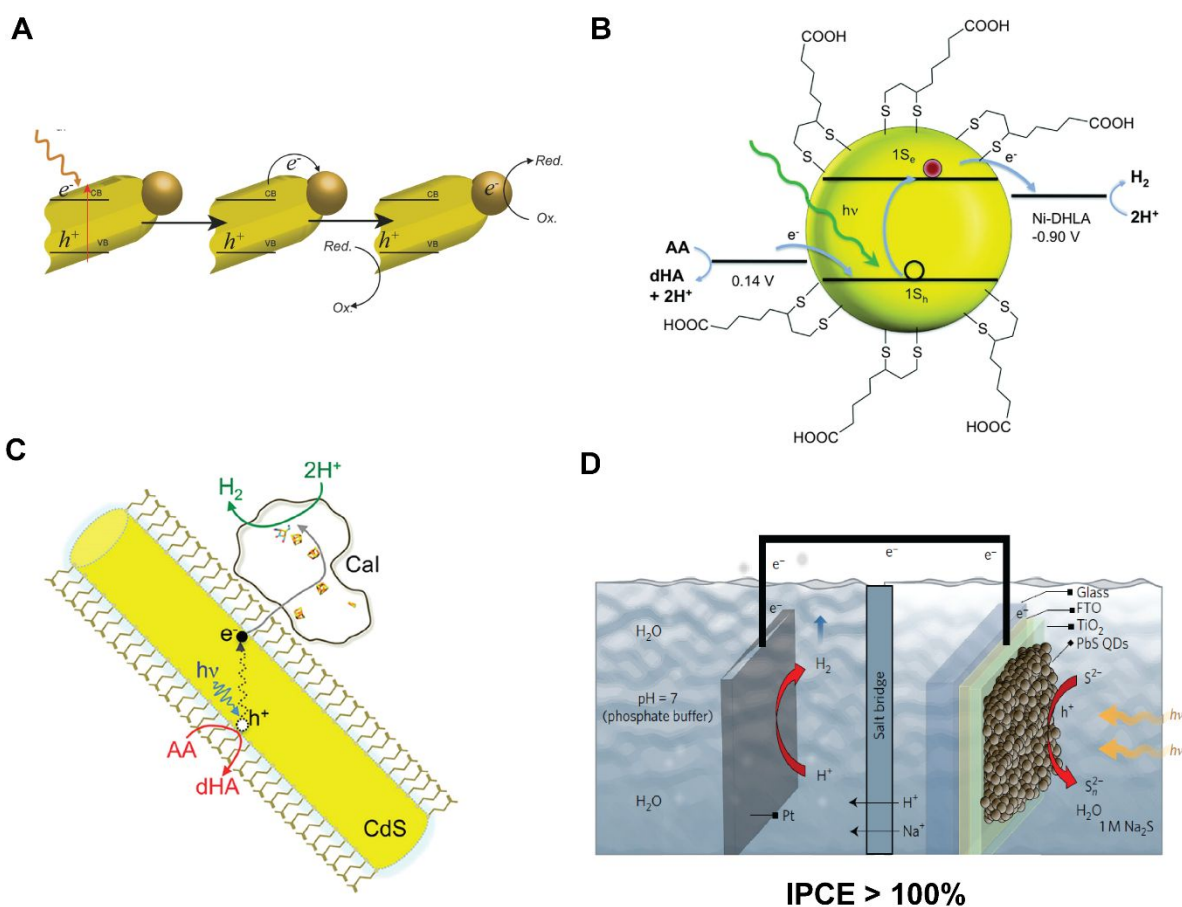


Figure 9. Four strategies of photon-driven H_2 production using QDs. (A) QDs with metal cocatalyst. (B) QDs with molecular cocatalyst. (C) QDs with hydrogenase or hydrogenase mimics. (D) Integrating QDs into photoelectrochemical cells. (A) was reproduced with permission from Ref. ¹⁵⁶. Copyright 2018 John Wiley and Sons. (B) was reproduced with permission from Ref. ¹⁵⁷. Copyright 2012, American Association for the Advancement of Science. (C) was reproduced with permission from Ref. ¹⁵⁸. Copyright 2012,

American Chemical Society. (D) was reproduced with permission from Ref. ¹⁵⁹. Copyright 2017, Nature Publishing Group.

4.1.1 QDs with Metal Cocatalyst

Traditionally, precious metals have been the most common cocatalysts with many semiconductors for photocatalytic hydrogen evolution.¹⁶⁰ The exact same strategy can be applied to QDs for hydrogen evolution, where photogenerated electrons in QDs are transferred to metal active sites, followed by transferring to protons. However, earlier reports using Pt-loaded CdS nanoporous structures,¹⁶¹ or platinized suspensions of cadmium zinc sulfide modified by silver sulfide,¹⁶² showed that these nanostructures are not photostable even though they displayed high apparent quantum yield of up to 60%. It is worth noting that the hydrogen evolution reaction is only a half reaction, and a hole scavenger is generally needed. The photo-instability is mainly due to the oxidizing holes that cause the oxidation of the chalcogen in QDs. Research in this field has been shifted to other nanostructures that attempt to separate the oxidizing holes within the structure, but progress remained rather slow until the synthetic challenges of preparing well-controlled nanorods and metal tips on nanorods had been addressed. In 2000, Alivisatos and co-workers^{163,164} reported colloidal synthesis of CdSe nanorods with well-controlled aspect ratios. Then in 2004, seminal work from Banin and co-workers¹⁶⁵ reported the selective growth of metal tips on various semiconductor nanorods and tetrapods by a simple reaction, where the size of nanorods and metal tips can be well controlled. Since then, the “nanorod-metal-tip” structure has become the prototype system for hydrogen generation. CdS nanorods, in conjunction with a Pt tip, have been the most common photocatalysts for hydrogen generation. To further prevent charge recombination upon photoexcitation, the wavefunction of electrons and holes can be engineered by preparing more complicated nanoheterostructures (*e.g.* Type II electronic structure). For instance, a Pt-tipped CdS nanorod with an embedded CdSe seed should be an ideal system for photocatalytic hydrogen evolution, as photogenerated electrons transfer to the metal tip while holes are localized to the CdSe seed.¹⁶⁶

However, the quantum efficiency for hydrogen evolution depends on many factors, including the size of the nanorod and seed, Pt particles, amount and combination methods of preparing the Pt particles. For instance, Amirav *et al.*¹⁶⁷ showed that both the length of the nanorod and size of CdSe seed affect the quantum efficiency of HER, and the optimized structure (60 nm long CdS rods, 2.3 nm CdSe seed and 3 nm Pt tip) exhibited 20% quantum efficiency under 450 nm illumination. Their nanorod heterostructure is 28 times more active for hydrogen generation compared to the unseeded rods, and the quantum efficiency remains the same for over 12 hours. The enhanced photostability is ascribed to physically separating the holes from the Pt/CdS interface. They further studied the photocatalytic activity dependence on the Pt loading amount.¹⁶⁸ Their report demonstrated that nanorods with only one Pt tip exhibited the highest hydrogen evolution efficiency with 27% apparent quantum yield, while nanorods with Pt particles on both tips displayed only 18% quantum yield. Heiz and co-workers¹⁶⁹ found that the size of Pt particles/clusters in CdS nanorods also plays an important role in the hydrogen evolution quantum

efficiency. The highest efficiency was obtained with Pt clusters containing an intermediate number of 46 atoms. The size effect is ascribed to the shift of LUMO level of Pt, which affects the electron transfer rate in both CdS to Pt and Pt to protons. In theory, the LUMO level of Pt should be low enough to accept electrons from CdS but at the same time high enough to transfer electrons to the molecular acceptor, namely protons. These two sequential steps are equally important for the hydrogen evolution efficiency.

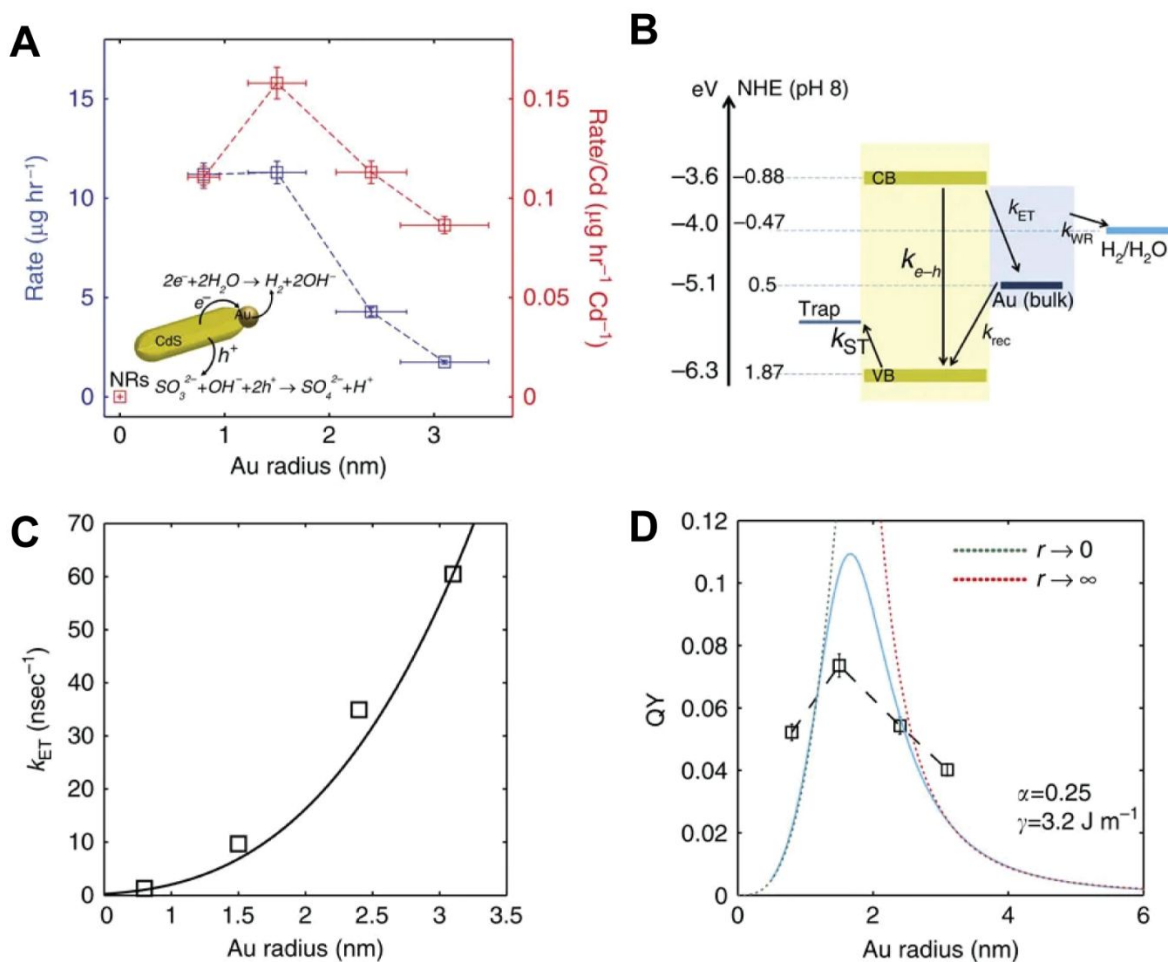


Figure 10. Size-dependent hydrogen generation yield in the CdS-Au system. (A) Hydrogen generation rate and cadmium normalized rate as a function of Au size. (B) Illustrative photocatalytic processes kinetic routes involved in hydrogen production. (C) Measured CdS-Au electron transfer rate and fitted curve using Fermi golden rule. (D) Measured quantum yield and the non-monotonic kinetic model. Reproduced from Ref¹⁷⁰. Copyright 2016, Nature Publishing Group.

The non-monotonic size dependence of the metal tips on the hydrogen evolution efficiency was recently studied in detail by Banin and co-workers¹⁷⁰ using a combination of transient absorption, hydrogen evolution kinetics, and theoretical modelling in a model system of CdS-Au nanorods (Figure 10). Their work shows that the size-dependent hydrogen evolution efficiency results from an interplay between the metal domain charging, the relative band alignments and the resulting

kinetics in this two-step reaction. The optimal size for the metal tip was explained in terms of two competing processes, namely the rate of electron transfer from CdS to metal tips and from metal tips to water. For small metal tips, the hydrogen evolution efficiency is mainly determined by the rate of electron injection to the metal tip; and for large metal tips, it is mainly determined by the water reduction on the metal surface. These two limits show opposite dependence on the metal size, leading to an intermediate size for the optimal value.

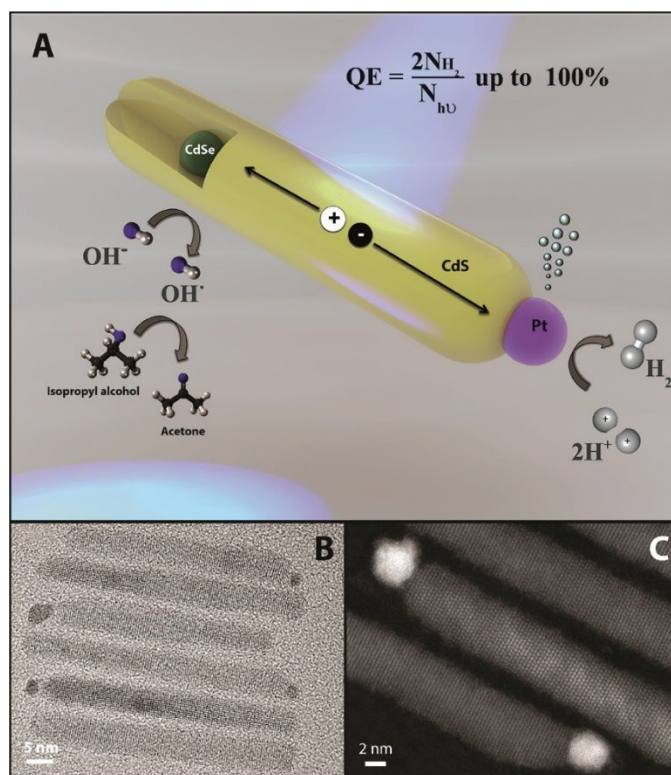


Figure 11. (A) Illustration of the photocatalytic hydrogen production process using Pt-tipped CdSe@CdS nanorods. Note that hydroxyl anion-radical redox couple was used as the redox mediator. (B) and (C) are TEM and high-resolution HAADF micrographs of Pt-tipped CdSe@CdS nanorods. A-C were reproduced with permission from Ref. ¹⁷¹. Copyright 2016 American Chemical Society.

Lately, researchers have focused on further optimizing the heterostructures,¹⁷²⁻¹⁷⁴ introducing new electron donors (hole scavengers), and understanding the charge separation dynamics and reaction mechanisms using ultrafast spectroscopic techniques. They find that the electron transport step is rapid and efficient, but the hole scavenging step is the efficiency-limiting step.^{173,175} Benefiting from this improved fundamental understanding, Amirav and co-workers¹⁷¹ combined the optimized Pt-tipped CdSe@CdS rods and hydroxyl anion-radical redox couple as the redox mediator, and were able to achieve a perfect photon-to-hydrogen quantum efficiency of 100% (Figure 11).

4.1.2 QDs with Molecular Cocatalyst

In addition to noble metals, molecular compounds in conjunction with QDs can also promote hydrogen evolution. Similar to metal cocatalysts, molecular compounds deliver electrons from photoexcited QDs to protons, acting as a photocatalytic active center. Such molecular catalytic centers can be found in transition metal ions (*e.g.* Ni^{2+} ,^{176,177} Co^{2+} ¹⁷⁸), complexes (metal ions with organic ligands)¹⁵⁷ or compounds (*e.g.* Co_2C ¹⁷⁹, MoP ¹⁸⁰, MoS_3 ¹⁸¹) and nanoclusters (*e.g.* $[\text{Mo}_3\text{S}_{13}]^{2-}$)¹⁸². For instance, by directly adding Co^{2+} ions into CdTe QD solutions, Wu and co-workers¹⁷⁸ showed that the photocatalytic hydrogen evolution activity can be significantly enhanced, with a turnover number of 219,100 based on QDs and hydrogen evolution rate of $25 \mu\text{mol h}^{-1} \text{mg}^{-1}$. Similar photocatalytic hydrogen evolution activity was also found in CdSe QDs with Ni^{2+} ions as the cocatalyst, and impressive progress has been made.^{176,177,183,184} Guo and co-workers¹⁸⁴ combined twinned $\text{Cd}_{0.5}\text{Zn}_{0.5}\text{S}$ nanocrystals and an unanchored NiS_x cocatalyst for hydrogen production, and they achieved an IQE of nearly 100% under 425 nm illumination with $\text{Na}_2\text{S}/\text{Na}_2\text{SO}_3$ as hole scavengers. Meanwhile, transition metal ions can also bind to surface organic ligands, forming molecular complexes as the photocatalytic center. In 2012, Eisenberg, Holland, Krauss and co-workers¹⁵⁷ found that CdSe QDs and dihydrolipoic-acid-complexed Ni^{2+} can act as robust and highly active photocatalysts for hydrogen generation (Figure 12A-B). Their photocatalyst gives > 600,000 turnovers based on the Ni complex and 1,200,000 based on the QDs at pH = 4.5 with ascorbic acid as the hole scavenger, and the activity remains unchanged for over 360 hours under illumination at 520 nm with a quantum yield of over 36%. They reported that the as-formed Ni complex is responsible for the high photocatalytic activity. They¹⁸⁵ further incorporated Co ions in the system and discovered that the Co-complex is much less efficient for hydrogen evolution. Recently, they expanded the family of metal complexes to a series of iron dithiolene complexes,¹⁸⁶ where they found that the overall order of activity correlates well with the reduction potential of the formally Fe(III) dimeric dianions. The effect of different capping ligands was also carefully studied.

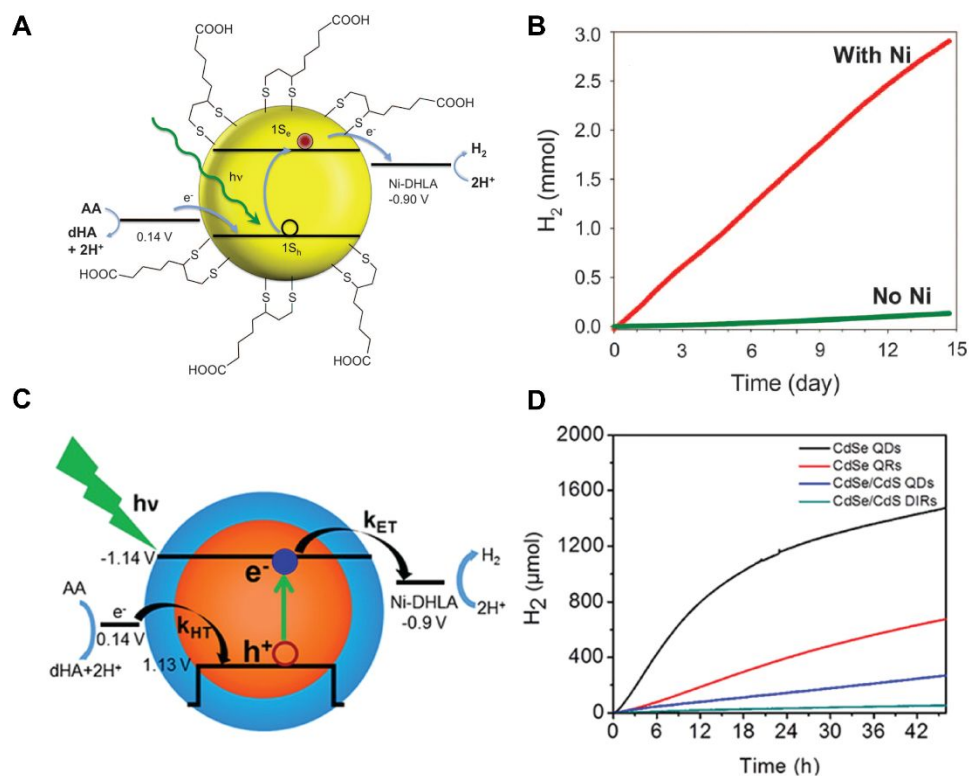


Figure 12. (A) Schematic diagram illustrating the photocatalytic H_2 production using CdSe QDs and Ni-DHLA as cocatalyst. (B) Hydrogen evolution over time using dihydrolipoic acid capped CdSe QDs with and without $\text{Ni}(\text{NO}_3)_2$. (C) Schematic diagram illustrating the photocatalytic H_2 production using CdSe/CdS core/shell QDs and Ni-DHLA as cocatalyst. (D) Hydrogen production over time using different nanostructures of QDs. A-B were reproduced with permission from Ref. ¹⁵⁷. Copyright 2012, American Association for the Advancement of Science. C-D were reproduced with permission from Ref. ¹⁸⁷. Copyright 2016, American Chemical Society.

Recent advances in this area are focusing on optimizing both the photosensitizer (*i.e.* QDs) and the molecular compounds and understanding the electron transfer mechanisms in the system. For instance, incorporating new QD heterostructures (*e.g.* core/shell, type I/II, Figure 12C-D)¹⁸⁷⁻¹⁸⁹ and surface capping ligands^{186,190-194} have led to both improved quantum efficiency and stability. Exploring new molecular catalysts is another interesting direction. Transition metal compounds (*e.g.* Co_2C ¹⁷⁹, MoP ¹⁸⁰, MoS_3 ¹⁸¹) and nanoclusters (*e.g.* $[\text{Mo}_3\text{S}_{13}]^{2-}$)¹⁸² are showing their potential in photocatalytic hydrogen evolution under visible-light illumination. Ultrafast spectroscopic results¹⁹⁵ have shown that electron transfer from the QDs to the molecular complexes is rapid and efficient, and thus is not the rate-limiting step; however, electron transfer from molecular complex to protons is rather sluggish, which should be further improved in the future.

4.1.3 QDs with Hydrogenase or Hydrogenase Mimics

Nature can convert protons to hydrogen in the dark using hydrogenase at the thermodynamic potential of the H^+/H_2 couple, with a rate of $6000\text{--}9000\text{ s}^{-1}$. Using natural hydrogenase as a cocatalyst with QDs as the light absorber thus represents a promising strategy for light-driven

hydrogen evolution. The challenge stems from the controlled assembly of QDs and hydrogenase in the right configuration (orientations, distances) so that the electron transfer rate is competitive with radiative and nonradiative recombination within the QDs. In 2010, King and co-workers¹⁹⁶ assembled CdTe QDs and *Clostridium acetobutylicum* [FeFe]-hydrogenase through electrostatic interactions, giving stable, enzymatically active complexes (Figure 13A). Using ascorbic acid as the sacrificial donor, they achieved an internal quantum efficiency of 9% under 532 nm illumination, and a turnover frequency of 25 s⁻¹. The internal quantum efficiency and turnover frequency were further improved to 20% and 983 s⁻¹ by coupling the same kind of hydrogenases to CdS colloidal nanorods (Figure 13B).¹⁵⁸ The enhanced catalytic activity was ascribed to a better electronic coupling between nanorods and hydrogenases, which leads to an accelerated electron transfer rate. Electron transfer kinetics between the CdS nanorods and hydrogenase were further studied in detail by Dukovic and co-workers.¹⁹⁷⁻¹⁹⁹ Their reports demonstrate that the electron transfer rate is comparable with the electron relaxation rate in CdS nanorods, both have values on the order of 10⁷ s⁻¹, and thus further optimization need to focus on increasing the electron transfer rate or decreasing the electron relaxation rate in nanorods.

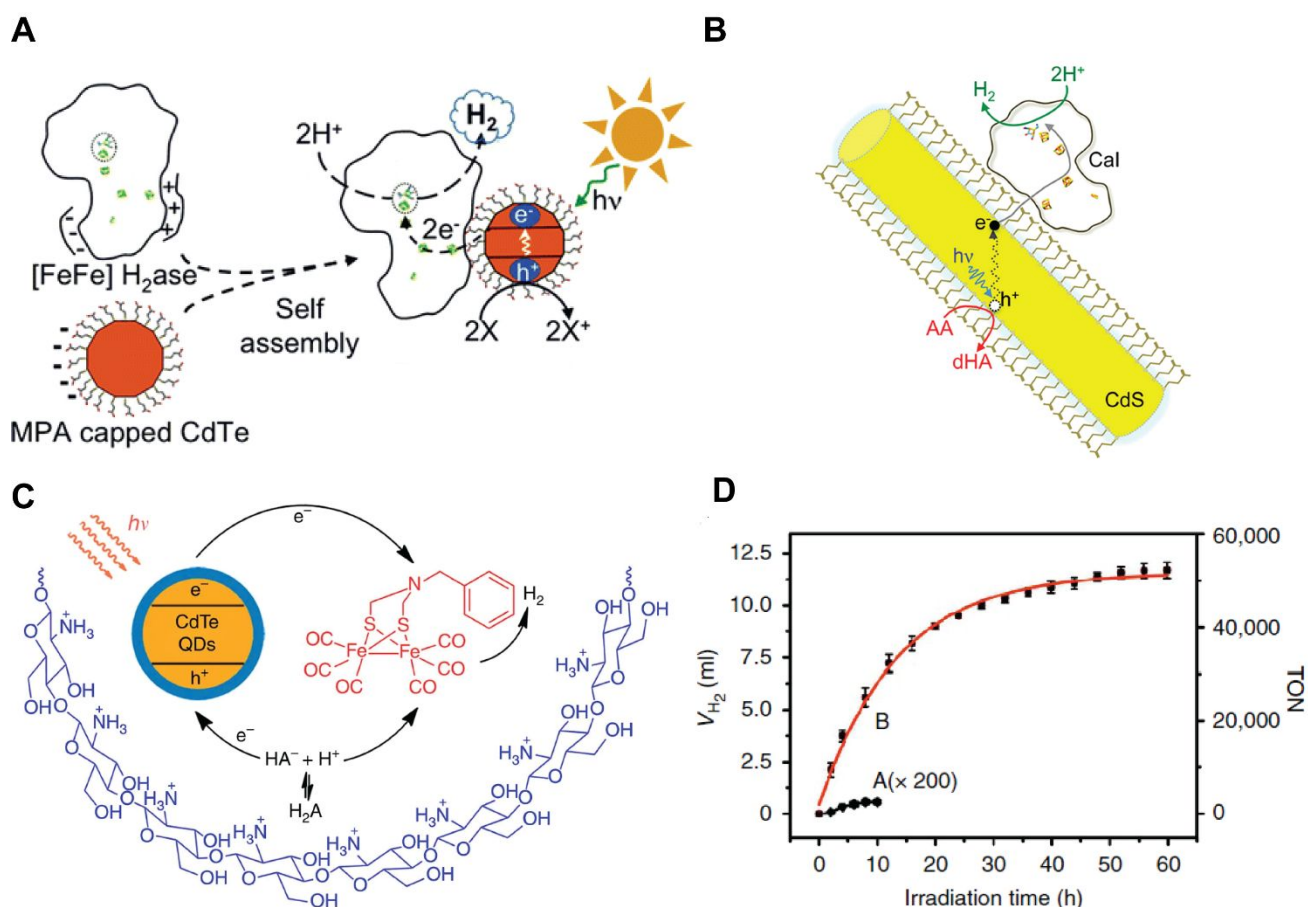


Figure 13. Schematic diagram illustrating the photocatalytic H₂ production using CdTe QDs (A) or CdS nanorods (B) coupled with [FeFe]-hydrogenase, and CdTe QDs coupled with hydrogenase mimics (C). (D) H₂ production using CdTe QDs- hydrogenase mimics in the absence (A) and presence (B) of chitosan. A

was reproduced from Ref. ¹⁹⁶. Copyright 2010, American Chemical Society. B was reproduced from Ref. ¹⁵⁸. Copyright 2012, American Chemical Society. C was reproduced from Ref. ²⁰⁰. Copyright 2013, Nature Publishing Group.

In addition to natural hydrogenases, hydrogenase mimics have also been incorporated with QDs for hydrogen evolution.²⁰¹ For instance, Wu and co-workers²⁰² coupled CdTe QDs with hydrophilic hydrogenase mimics to achieve a turnover number of 505 for hydrogen production. The quantum efficiency and turnover number were further improved dramatically by introducing chitosan into the QD-hydrogenase mimic system to simulate the confined environment around the active site of hydrogenase in nature (Figure 13C-D).²⁰⁰ With this strategy, they improved the turnover number to 5.28×10^4 . In addition to CdTe QDs, CdSe QDs have also been explored as couple with hydrogenase mimics, showing impressive photon-to-H₂ quantum efficiencies.^{203,204}

4.1.4 Integrating QDs into Photoelectrochemical Cells

Another interesting paradigm is to assemble QDs into QD-solids that then form photoelectrodes in photoelectrochemical cells. In this configuration, photogenerated electrons and holes can be physically separated similar to a solar cell architecture. When the cathode is immersed into an aqueous solution, light-driven H₂ evolution can occur. In 2017, Beard and co-workers¹⁵⁹ developed photoelectrochemical cells based on PbS QDs that can produce H₂ from aqueous Na₂S solutions (Figure 14A-B). In their system, one electrode consists of a PbS QD layer deposited onto FTO/TiO₂ and served as a photoanode. The photoanode is immersed into an aqueous Na₂S solution (1M) and electrically connected to a dark electrode, Pt, that is submersed in a phosphate buffer (pH = 7) in a separate compartment. The two compartments are connected by a salt bridge to complete the circuit. Upon photoexcitation, PbS QD layer generates electron-hole pairs, the photogenerated holes oxidize sulfide ions (S²⁻) at the PbS QD/Na₂S solution interface, while photogenerated electrons are relayed to the Pt electrode where they reduce H⁺ to H₂. Therefore, the overall reaction is to photosplit H₂S and generates H₂. Since the integrated PbS QDs undergo MEG (discussed above), generating 2 excitons (electron-hole pairs) per photon absorbed for high energy photons, they successfully generated H₂ with a peak external quantum efficiency (photons-to-H₂) of up to 120% (Figure 14D). They demonstrated that efficient MEG was triggered when the incident photon energy is larger than 2.7 times of the PbS QD bandgap energy. Their results suggest that QDs possess a tremendous potential to achieve high-efficiency production of solar fuels. Moving forward, coupling the photoanode with a photocathode to increase the generated photovoltage is needed in order to extend the H₂S splitting reaction based on QDs arrays to the production of H₂ directly from water splitting. Beard and co-workers calculated, based upon the detail-balance approach, that the water-splitting power conversion efficiency can greatly benefit from MEG when a small amount of solar concentration (10-100x) is also employed.²⁰⁵

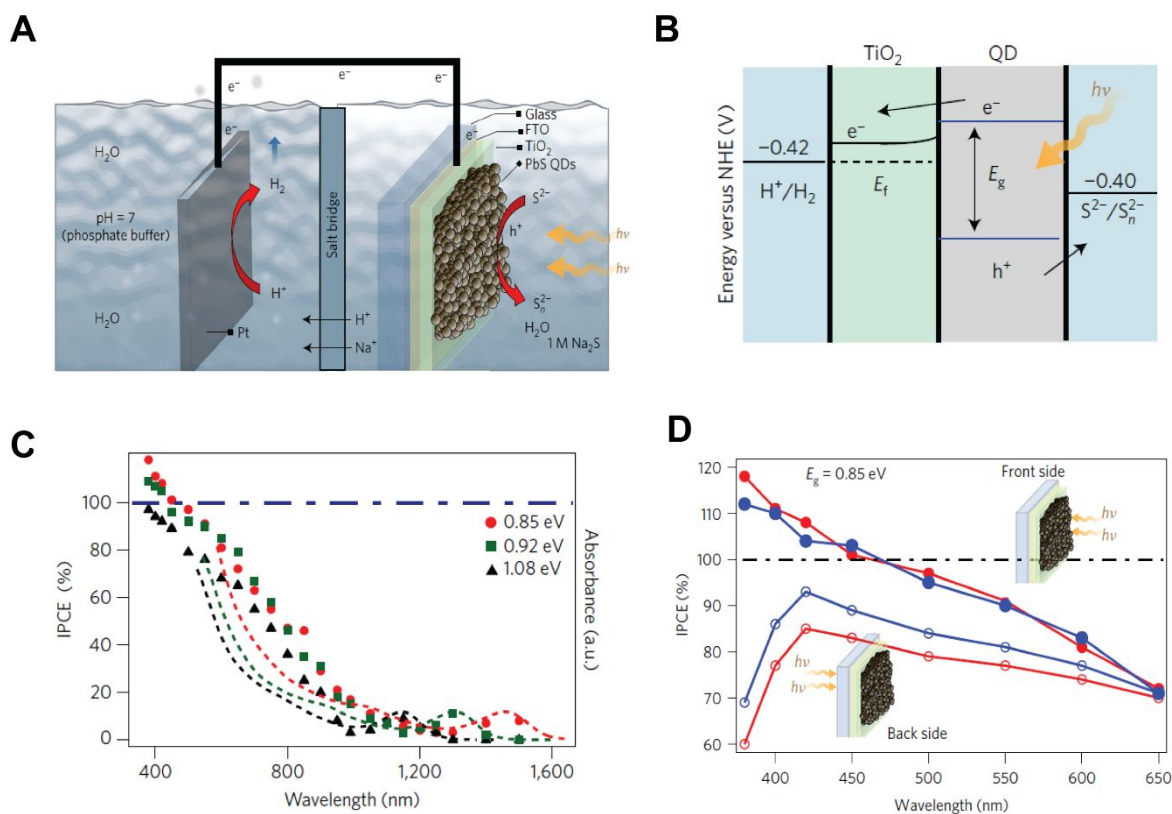


Figure 14. (A) Schematic illustration of the photoelectrochemical cell based on PbS QDs to produce H₂. (B) Energy diagram of QDs, TiO₂, and redox chemical potentials. (C) IPCE of PbS QDs with different sizes. Over 100% IPCE was observed in smaller QDs (E_g: 0.92 and 0.85 eV). (D) Comparison of the IPCE for front and back illuminations based on PbS QDs (E_g: 0.85 eV). Reproduced from Ref. ¹⁵⁹. Copyright 2017, Nature Publishing Group.

4.2 C-C, C-O, and C-N Bonds Formation

Although the apparent photon-to-H₂ quantum efficiency was improved to nearly 100% based on QD systems, a sacrificial agent or a cocatalyst is generally required, and QDs do not serve as the catalytic center in most cases. In addition, using QDs as photocatalysts for useful organic synthesis, such as C-C, C-O and C-N bond formation remained a challenge until recent progress demonstrated the utility to this approach. In 2017, Weiss and co-workers²⁰⁶ demonstrated that colloidal CdS QDs can be used by themselves to photocatalyze a C-C coupling reaction between 1-phenylpyrrolidine (PhPyr) and phenyl trans-styryl sulfone (PhSO₂). They proposed that the C-C coupling is mediated through a radical-radical coupling mechanism, and the QDs serve as a photoredox catalysts to transfer both photoinduced electrons and holes separately to the different molecular substrates (Figure 15A). Specifically, photoexcitation by 405 nm light generates excited state QDs, which subsequently transfer holes to PhPyr, generating a reduced QD and an amino radical **2**. The amino radical can then attack the double bond in PhSO₂ after deprotonation, forming the sulfonyl radical **4**. Finally, **4** accepts electrons from the reduced QDs and eliminates the PhSO₂⁻ ion, forming the product **5** and closing the cycle. They further found that the photoinduced hole

transfer from QDs to PhPyr is the rate-limiting step, which can be modulated by the optimization of the QD-ligand shell. The generality of C-C bond formation using QDs as photocatalysts was also investigated by Krauss, Weix and co-workers⁸ almost at the same time as the Weiss study. Their report found that CdSe QDs can be employed to photocatalyze five different organic reactions, including β -alkylation, β -aminoalkylation, amine arylation, dehalogenation, and decarboxylative radical formation (Figure 15B-C). A library of C-C and C-N coupling reactions between aldehydes/ketones and olefins/amines were achieved to yield alkylation, aminoalkylation, and amine arylation products with moderate to high reaction yields. Without further optimization of the QDs or the reaction conditions, reaction efficiencies based on CdSe QDs are revealed to be comparable to the best available molecular metal dyes. Additionally, their CdSe QD photocatalyst can tolerate a variety of potential poisons, ligands, organic cocatalysts, and transition-metal cocatalysts. Soon after, König and co-workers²⁰⁷ showed that ZnSe/CdS QDs can be used for reductive dehalogenations and C-H arylation reaction from aryl bromides. They also proposed that the reaction is mediated through a radical-radical coupling mechanism.

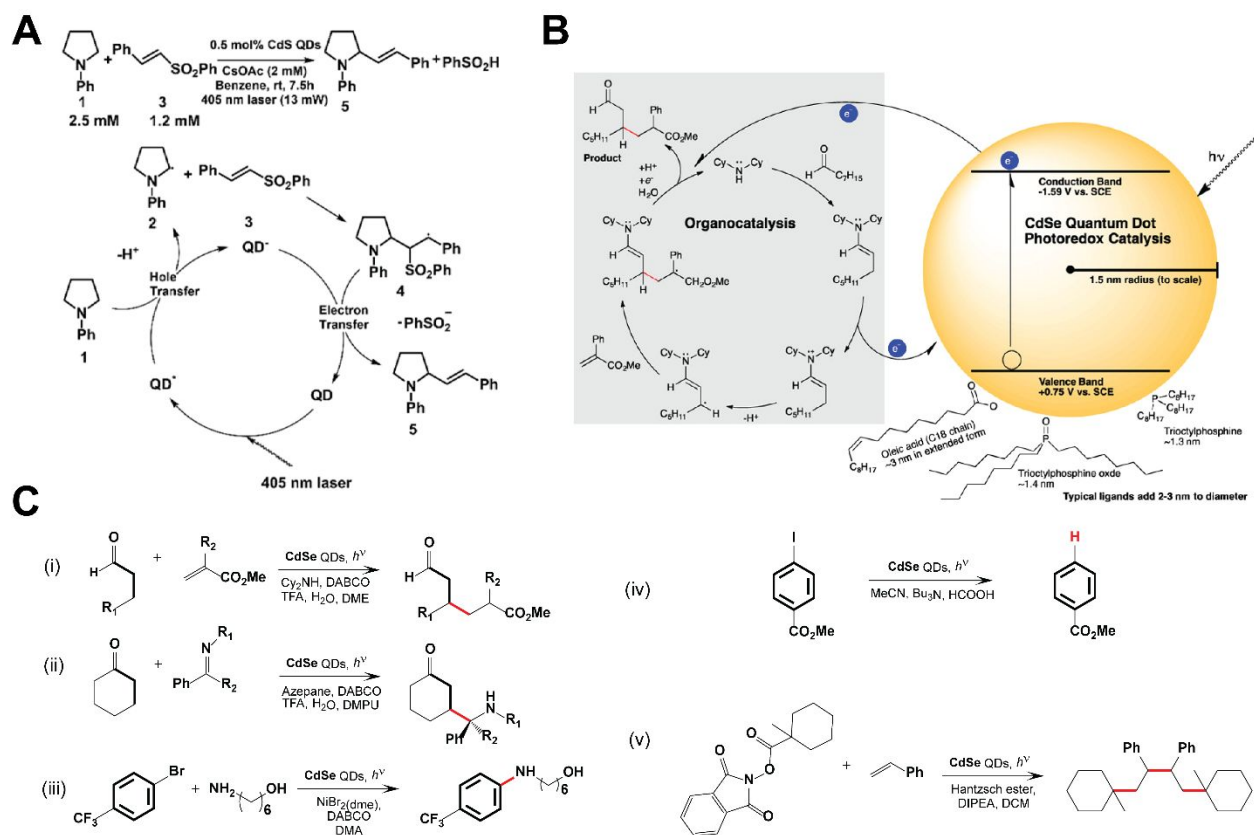


Figure 15. Proposed reaction mechanism for C-C coupling reaction of 1-phenylpyrrolidine and phenyl trans-styryl sulfone (A), and β -alkylation (B). (C) Photocatalytic cross coupling reactions reported from Ref. 8. (A) was reproduced from Ref. 206. Copyright 2017, American Chemical Society. (B-C) were reproduced from Ref. 8. Copyright 2017, American Chemical Society.

Recently, Yan and co-workers⁷ demonstrated that CsPbBr₃ perovskite nanocrystals can selectively photocatalyze another C-C formation reaction, namely α -alkylations, with a turnover number of

over 52,000 under visible light illumination (Figure 16A). Subsequently, they expanded the reaction scope to C-N and C-O bond formations via N-heterocyclizations and aryl-esterifications with moderate to high reaction yields (Figure 16B).²⁰⁸ In addition, they find that large size perovskite nanocrystals generally display higher reaction yields compared to smaller QDs, which they attribute to a stability issue (larger nanocrystal being more stable than smaller ones). Perovskite nanocrystals also apparently provide higher reaction activity in air than most of the developed photocatalysts because of a higher air tolerance for the perovskite nanocrystal. For instance, when compared to traditional II-VI QDs (CdSe) or molecular catalysts ($\text{Ru}(\text{bpy})_3(\text{PF}_6)_2$, $\text{Ir}(\text{ppy})_3$), CsPbBr_3 nanocrystals generally exhibit higher reaction yields and turnover numbers. Their study demonstrates the generality of perovskite nanocrystals or QDs for a broad scope of organic synthesis. A subsequent reaction mechanism study²⁰⁹ by transient absorption spectroscopy revealed that the reaction is initiated by an ultrafast charge transfer, forming a charge separated state with $\sim 0.8 \mu\text{s}$ lifetime. This near microsecond charge separated state allows the photogenerated charged radical intermediates to form C-C bonds in a biradical pathway, but the lifetime is not long enough to support chain propagation. However, it still remains an open question if this biradical pathway is generic reaction pathway for QDs-based photocatalytic reactions.

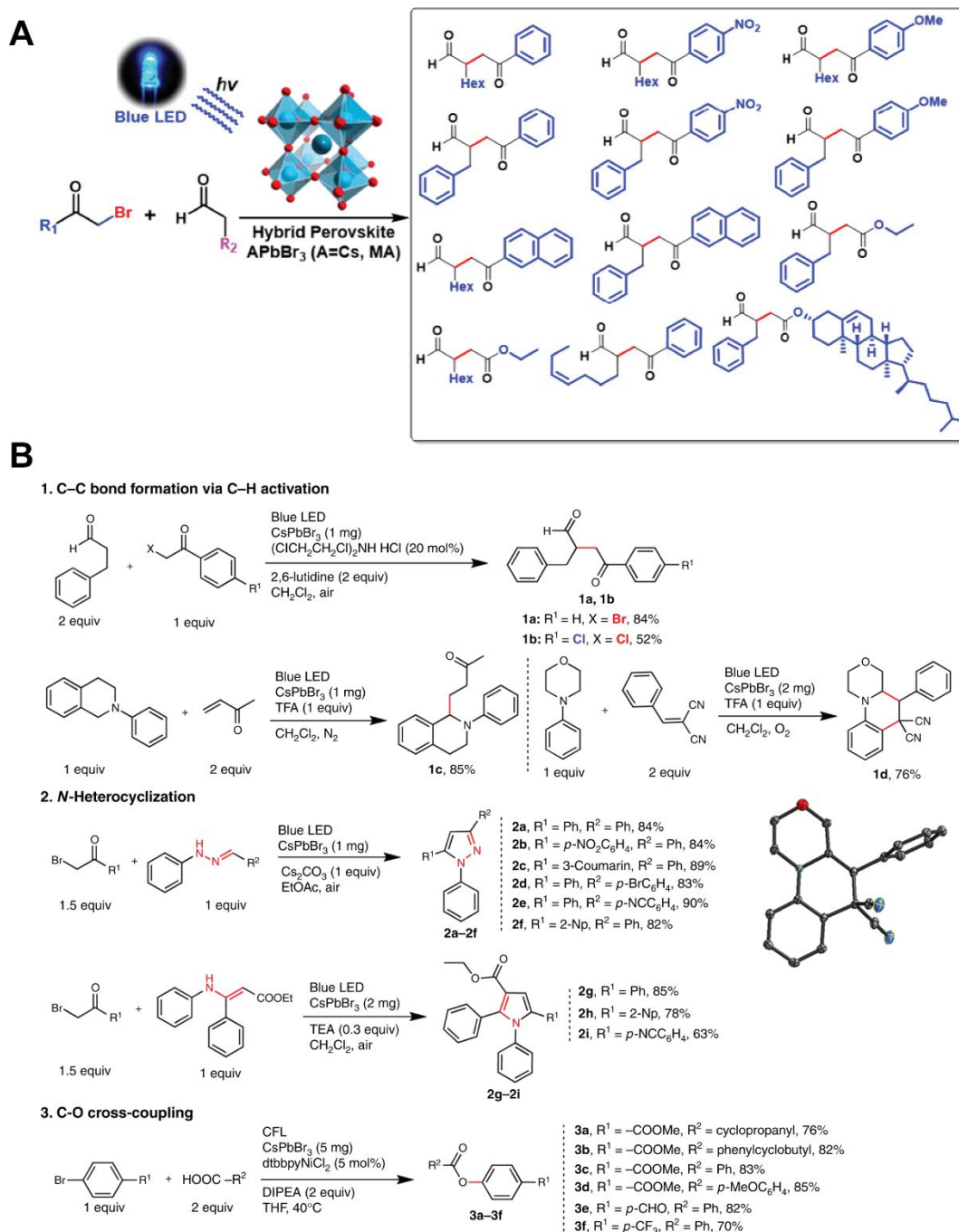


Figure 16. Photocatalytic α -alkylation of aldehydes (A), N-heterocyclizations and aryl-esterifications (B) enabled by CsPbBr₃ nanocrystals. (A) was reproduced from Ref. 7. Copyright 2019, American Chemical Society. (B) was reproduced from Ref. 208. Copyright 2019, Nature Publishing Group.

In addition to the above-mentioned benefits of QDs as a photocatalyst for organic synthesis, Weiss and co-workers⁹ recently demonstrated that QDs can bring unique opportunities for the regio- and diastereoselective organic synthesis due to a QD surface effect. They employed CdSe QDs as visible-light photocatalysts for homo- and hetero-intermolecular [2+2] photocycloadditions of 4-

vinylbenzoic acid derivatives with up to 98% switchable regioselectivity and 98% diastereoselectivity for *syn*-cyclobutane products that are previously unattainable using traditional methods. Using transient absorption spectroscopy, they demonstrated that the photocatalytic reaction was triggered by efficient triplet-triplet energy transfer from QDs to the molecular surface bound substrates. With the mechanism, they further found that they can obtain selective heterocoupling, apart from homocoupling, by precisely controlling the triplet energy level of the QDs. The excellent diastereoselectivity and tunable regioselectivity was attributed to the surface “templating” effect, where molecular substrates can reversibly absorb and desorb through carboxylic ligands (Figure 17). Therefore, their study demonstrated that QDs not only can provide exceptional activity towards a variety of organic synthesis, but also present a new strategy to achieve high diastereoselectivity and regioselectivity for the development of more complicated industrial-relevant drug molecules.

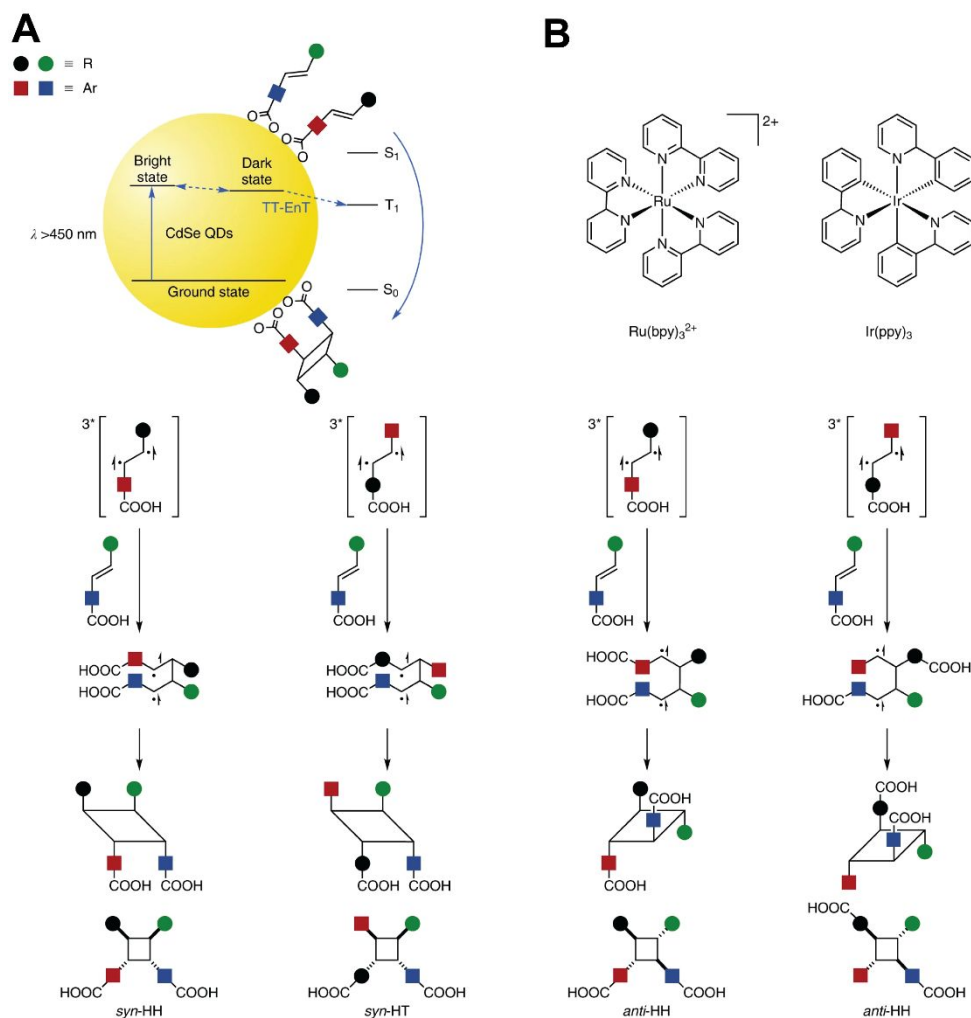


Figure 17. (A) Triplet sensitization of organic substrates via the QD photocatalyst and the mechanisms of *syn*-HH selectivity for [2+2] photocycloadditions. (B) Sensitization of organic substrates via the molecular sensitizers and the mechanism of the *anti*-HH selectivity for [2+2] photocycloadditions. Reproduced with permission from Ref. 9. Copyright 2019, Nature Publishing Group.

4.3 Other Multielectron Chemical Transformation

4.3.1 CO₂ Reduction

CO₂ photoreduction is a promising strategy to close the carbon cycle and to construct a sustainable society. Similar to the scenario in H₂ generation (Section 4.1), colloidal QDs can couple with a cocatalyst (*e.g.* metal,²¹⁰⁻²¹² metal oxides,²¹³ and molecular complexes²¹⁴⁻²¹⁶) to reduce CO₂ under light irradiation. In these cases, semiconductor QDs only work as a photosensitizer, which delivers photogenerated electrons to the cocatalyst that subsequently reduces CO₂. Initial reports for CO₂ photoreduction are mainly focused on traditional cadmium chalcogenide QDs (CdS, CdSe, CdTe).²¹⁷ Recently, ternary colloidal QDs including CuInS₂ and perovskite QDs are being investigated as intriguing potentials for photocatalytic CO₂ reduction. In 2018, Weiss and co-workers²¹⁸ coupled charged CuInS₂/ZnS QDs with trimethylamino-functionalized iron tetraphenylporphyrin (FeTMA) as cocatalysts for CO₂ photoreduction. With optimal conditions, they achieved a turnover number of 450 per catalyst after 30 h illumination of 450 nm light and a selectivity for CO product of 99% (Figure 18A). Ultrafast spectroscopy studies revealed that electron transfer from multiple QDs to a single FeTMA can be very efficient (~100%), and the sensitization efficiency is 11 times greater than that of the physical mixture of QD/FeTMA in DMSO. Tian and coworkers²¹⁹ covalently linked CuInS₂ QDs with a molecular Re cocatalyst. They found that the covalent linkage aids the ultrafast electron transfer from QDs to Re catalyst, which leads to an enhanced photocatalytic activity for CO₂ reduction to CO. They subsequently deposited the QDs/Re catalyst onto NiO photocathode, forming a photoelectrochemical cell for CO₂ reduction.²²⁰ With this configuration, they achieved a faradaic efficiency of 32% for CO production. Reisner and co-workers²¹⁴ anchored CdS QDs with non-precious molecular nickel terpyridine complexes, which photocatalyzed CO₂ reduction with >90% selectivity under UV-filtered simulated solar light irradiation. Their results demonstrate that anchoring the molecular Ni catalyst on the QD surface is key in controlling the selectivity for CO₂ reduction over H₂ evolution in aqueous solutions. Interestingly, for some other QDs, a cocatalyst is not necessary for CO₂ photoreduction and these QDs work as both photosensitizer and catalyst. For instance, in 2017, Sun and co-workers²²¹ found that CsPbBr₃ QDs, by themselves, can photo-reduce CO₂ with over 99% selectivity (towards CO) and an efficient yield of 20.9 μmol h⁻¹ upon light irradiation. Several other reports²²²⁻²²⁵ also demonstrated high selectivity and activity for photocatalytic CO₂ reduction based on MA/CsPbBr₃ QDs, suggesting the superior photocatalytic activity of these systems. However, it is worth noting that the efficiency and selectivity for photocatalytic CO₂ reduction based on QDs are still relatively low, especially for usable fuels and value-added chemicals (*i.e.* C₂+ products). So far, almost all QD systems produce C₁ products. While C₂+ products are generally more valuable, it still remains a significant challenge to generate them photocatalytically. Therefore, future research should focus on exploring the opportunities for selectively generating C₂+ products, improving the product selectivity, and deepening the understanding of reaction mechanism in CO₂ reduction based on QDs.

4.3.2 N₂ Fixation

QDs have also been explored for photocatalytic N_2 reduction. The strategy is again very similar to H_2 generation or CO_2 reduction, that is couple the QDs that absorb the light with a good cocatalyst to reduce N_2 under light irradiation. However, here the challenge stems from the limited choices of cocatalysts that can reduce N_2 efficiently. When hydrogenase is replaced with nitrogenase, QDs can be employed to drive the photoreduction of N_2 . In 2016, King and co-workers²²⁶ assembled CdS nanorods and nitrogenase MoFe protein and realized photocatalytic N_2 reduction under 405 nm light illumination (Figure 18B-C). Similar to the QD-hydrogenase system, CdS nanorods work as light harvesters, and they photosensitize the nitrogenase MoFe protein to drive the enzymatic reduction of N_2 into NH_3 . In such a way, the photon energy harvested by the QDs can effectively replace the chemical energy from adenosine 5'-triphosphate (ATP) hydrolysis in the biological system. Under optimal conditions, they obtained a turnover rate of 75/min and 63% of the ATP-coupled reaction rate for nitrogenase complex. Their study demonstrated the vast potential of QD-enzyme biohybrids for light-driven chemical transformations. Learning from the success of the QD-based H_2 production and CO_2 reduction, we envision that future success in photocatalytic N_2 reduction will come from the development of both novel QDs and cocatalyst, the optimized interaction between the QDs and the cocatalysts, and an in-depth understanding of the reaction mechanisms. For instance, since the emerging family of perovskite QDs (*e.g.* $CsPbBr_3$) has driven some recent breakthroughs in photocatalytic reactions, it could be fruitful to explore perovskite QDs for N_2 reduction reactions.

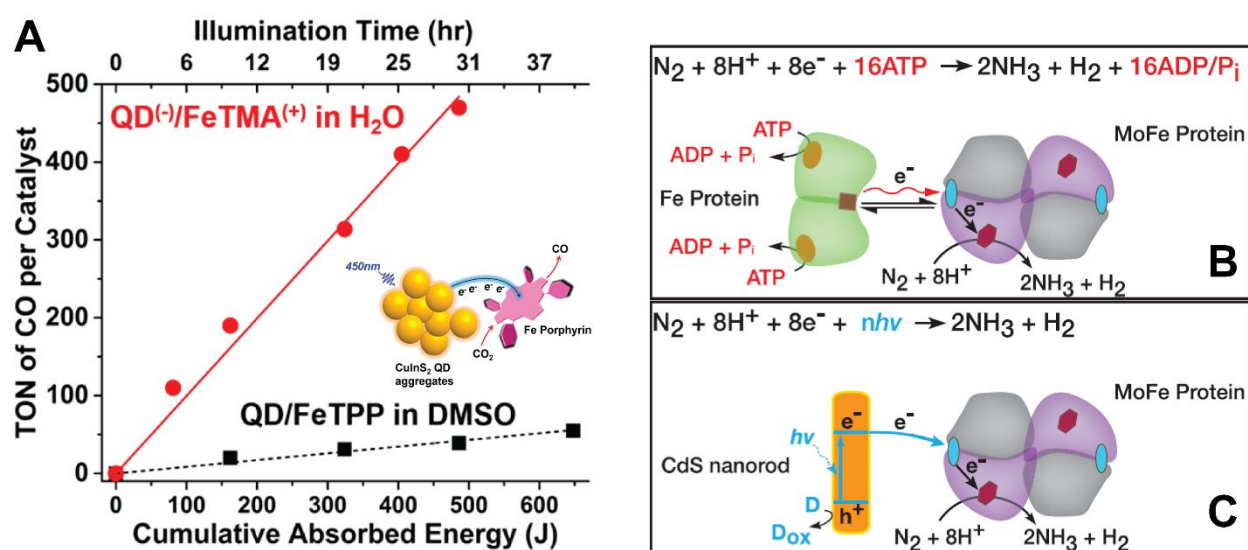


Figure 18. (A) Photocatalytic CO_2 reduction using QD/FeTMA: TON as a function of absorbed photon energy. Reproduced from Ref. ²¹⁸. Copyright 2018, American Chemical Society. (B-C) Schematic illustration of N_2 reduction to NH_3 by nitrogenase driven by ATP (B) and CdS:MoFe protein biohybrids (C). Reproduced from Ref. ²²⁶. Copyright 2016, The American Association for the Advancement of Science.

5. Conclusions and Outlook

In this review, we highlight recent advances in using colloidal QDs for absorbing, manipulating and directing the flow of optical energy into other useful forms of energy. The advantages of QDs

compared to molecular chromophores in converting optical energy to electron energy, to other wavelengths of light, and to chemical bonds are the focus and frame the discussion. First, we described how QDs can be implemented into solar cells to convert optical energy to electricity, highlighting the opportunity of overcoming the SQ limit by taking advantage of the MEG process. We then summarized recent progress in photon up- and down-conversion approaches based on colloidal QDs. Finally, we discussed recent advances of using QDs for photocatalytic chemical conversion, including hydrogen evolution, CO₂ reduction, N₂ reduction, and organic coupling reactions.

Assembled QD arrays are able to effectively convert solar energy to electricity. The past decade has witnessed a continuing and steady progress in QDPV, with the power conversion efficiencies that are approaching other solution-processable photovoltaic technologies (*e.g.* organic solar cells). Quantum yields exceeding 100% *via* MEG has been demonstrated in working QD solar cells, showing great promise in the quest to bypass the SQ limit for single-junction solar cells. However, further improvement in the MEG efficiency at lower energy thresholds requires careful synthetic control towards more advanced heterostructures (both for the inorganic core and organic ligand shell²²⁷), which can effectively slow down the cooling rates of hot-carriers due to additional channels. As such, advanced QD nanostructures²²⁸ should continue to be explored for further MEG improvements. Shape, composition, and heterostructure effects are underexplored and provide avenues for exploration. As an example, very high MEG results were recently reported in 2D MoTe₂.²²⁹ Understanding and controlling the electronic interactions between QDs (QD-QD electronic coupling), and QD-ligands, that can lead to high carrier mobilities, low trap densities, and long carrier lifetimes without losing the beneficial impacts of quantum-confinement will lead to breakthroughs that in turn can further improve QDPVs. All of these efforts are closely tied with the development of new synthetic methods and QD-film processing in order to prepare monodispersed,²³⁰ well-defined QD arrays or superstructures, where ligand coordination chemistry can play an extremely important role. The connections between synthesis, QD-monodispersity, trap density, QD performance, etc., need to be better understood. Apart from QD structure, device engineering can also accelerate the development of QDPV, in particular those architectures that take advantage of the unique aspects of QDs.

Recently, QDs are also finding new opportunities in photon up- and down-conversion mediated through electronic coupling with organic chromophores and quantum cutting. However, several challenges exist and limit these platforms for practical use. For example, most of the QDs mentioned above contain lead or cadmium. The toxic heavy metals are not environmentally friendly and limit their use in biological systems (especially for photon up-conversion). The development of non-toxic systems, for instance, Si QDs,²³¹ which are free of heavy metals could yield significant benefits. The community should continue exploring the electronic coupling between inorganic QDs and organic chromophores in a broader material scope. Additionally, reabsorption would be a challenge in triplet fusion based up-conversion due to the strong absorptivity of the QDs in the spectrum of the up-converted emission. Minimizing the thickness

of the thin film could be a solution. For quantum cutting with lanthanide ions doped into perovskite QDs, the mechanism is proposed as a trap state mediated two sequential energy transfer from conduction band of the QDs to the lanthanides. Detailed studies should provide a better understanding of the nature of this trap state and the energy transfer process. Furthermore, a careful study of the apparent lock-and-key relationship between perovskite QDs and Yb³⁺ ions in the quantum cutting process is needed, as no quantum cutting has been observed in other Yb³⁺ doped QDs, or perovskite QD doped with other lanthanide ions.

QDs-based hydrogen evolution has achieved great progress, reaching 100% apparent photon-to-hydrogen efficiency based on the nanorod-metal-tip system. Other multi-electron transformations (*e.g.* CO₂ and N₂ reduction) based on QDs with cocatalysts have also been demonstrated, exhibiting quantum efficiencies comparable to other photosensitizers, such as organic chromophores. To further improve the quantum efficiency, new QDs nanostructures, cocatalysts, and sacrificial agents need to be explored and optimized. Ultrafast reaction dynamics can shed light on the mechanisms and thus ultimate potential.¹⁶⁶ Recent advances in photocatalytic organic synthesis using QDs as the photocatalyst is extremely intriguing and exciting. However, the generality of organic coupling reactions based on QDs as photocatalysts should be further investigated, and the reaction mechanisms needs to be better understood and controlled. Computational,²³²⁻²³⁴ in conjunction with ultrafast spectroscopic²⁰⁹ techniques could bring tremendous value in understanding the reaction mechanism (*e.g.* key reaction intermediates, pathways, origin of chemo-selectivity, and reaction time scales). Apart from the high quantum efficiency, QD-based photocatalytic systems also possess unique opportunities towards regio- and diastereoselective organic synthesis. Another interesting direction that can be foreseen is to use QDs as a photocatalysts for enantioselective organic synthesis. Overall, colloidal QDs have emerged as an efficient scaffold to transduce optical energy to electricity, to other wavelengths of light, and to chemical bonds, and further development of quantum-confined systems is likely to greatly benefit emerging energy technologies.

Acknowledgement

We thankfully acknowledge support for this work through the solar photochemistry program within the Division of Chemical Sciences, Geosciences, and Biosciences, Office of Basic Energy Sciences, Office of Science within the U.S. Department of Energy through Contract No. DE-AC36-08G028308. Work on perovskite systems is supported as part of the Center for Hybrid Organic Inorganic Semiconductors for Energy (CHOISE) an Energy Frontier Research Center funded through the office of Basic Energy Sciences, Office of Science, within DOE. The views expressed in the article do not necessarily represent the views of the DOE or the U.S. Government. The U.S. Government retains and the publisher, by accepting the article for publication, acknowledges that the U.S. Government retains a nonexclusive, paid-up, irrevocable, worldwide license to publish or reproduce the published form of this work, or allow others to do so, for U.S. Government purposes.

References

- (1) National Renewable Energy Laboratories. *Best research-cell efficiencies 2019*, <https://www.nrel.gov/pv/cell-efficiency.html>.
- (2) Nozik, A. J.; Beard, M. C.; Luther, J. M.; Law, M.; Ellingson, R. J.; Johnson, J. C. Semiconductor Quantum Dots and Quantum Dot Arrays and Applications of Multiple Exciton Generation to Third-Generation Photovoltaic Solar Cells. *Chemical Reviews* **2010**, *110*, 6873-6890.
- (3) Pan, G.; Bai, X.; Yang, D.; Chen, X.; Jing, P.; Qu, S.; Zhang, L.; Zhou, D.; Zhu, J.; Xu, W.; Dong, B.; Song, H. Doping Lanthanide into Perovskite Nanocrystals: Highly Improved and Expanded Optical Properties. *Nano Letters* **2017**, *17*, 8005-8011.
- (4) Milstein, T. J.; Kroupa, D. M.; Gamelin, D. R. Picosecond Quantum Cutting Generates Photoluminescence Quantum Yields Over 100% in Ytterbium-Doped CsPbCl₃ Nanocrystals. *Nano Letters* **2018**, *18*, 3792-3799.
- (5) Fan, X.-B.; Yu, S.; Hou, B.; Kim, J. M. Quantum Dots Based Photocatalytic Hydrogen Evolution. *Israel Journal of Chemistry* **2019**, *59*, 762-773.
- (6) Huang, C.; Li, X.-B.; Tung, C.-H.; Wu, L.-Z. Photocatalysis with Quantum Dots and Visible Light for Effective Organic Synthesis. *Chemistry – A European Journal* **2018**, *24*, 11530-11534.
- (7) Zhu, X.; Lin, Y.; Sun, Y.; Beard, M. C.; Yan, Y. Lead-Halide Perovskites for Photocatalytic α -Alkylation of Aldehydes. *Journal of the American Chemical Society* **2019**, *141*, 733-738.
- (8) Caputo, J. A.; Frenette, L. C.; Zhao, N.; Sowers, K. L.; Krauss, T. D.; Weix, D. J. General and Efficient C–C Bond Forming Photoredox Catalysis with Semiconductor Quantum Dots. *Journal of the American Chemical Society* **2017**, *139*, 4250-4253.
- (9) Jiang, Y.; Wang, C.; Rogers, C. R.; Kodaimati, M. S.; Weiss, E. A. Regio- and diastereoselective intermolecular [2+2] cycloadditions photocatalysed by quantum dots. *Nature Chemistry* **2019**, *11*, 1034-1040.
- (10) Shockley, W.; Queisser, H. J. Detailed Balance Limit of Efficiency of $p-n$ Junction Solar Cells. *Journal of Applied Physics* **1961**, *32*, 510-519.
- (11) Nozik, A. J. Quantum dot solar cells. *Physica E* **2002**, *14*, 115-120.
- (12) Schaller, R. D.; Klimov, V. I. High Efficiency Carrier Multiplication in PbSe Nanocrystals: Implications for Solar Energy Conversion. *Physical Review Letters* **2004**, *92*, 186601.
- (13) Beard, M. C.; Midgett, A. G.; Hanna, M. C.; Luther, J. M.; Hughes, B. K.; Nozik, A. J. Comparing multiple exciton generation in quantum dots to impact ionization in bulk semiconductors: Implications for enhancement of solar energy conversion. *Nano Lett.* **2010**, *10*, 3019.
- (14) Hanna, M. C.; Beard, M. C.; Nozik, A. J. Effect of Solar Concentration on the Thermodynamic Power Conversion Efficiency of Quantum-Dot Solar Cells Exhibiting Multiple Exciton Generation. *J. Phys. Chem. Lett.* **2012**, *3*, 2857-2862.
- (15) Beard, M. C.; Luther, J. M.; Semonin, O. E.; Nozik, A. J. Third Generation Photovoltaics based on Multiple Exciton Generation in Quantum Confined Semiconductors. *Accounts of Chemical Research* **2013**, doi: 10.1021/ar3001958.
- (16) Boriskina, S. V.; Green, M. A.; Catchpole, K.; Yablonovitch, E.; Beard, M. C.; Okada, Y.; Lany, S.; Gershon, T.; Zakutayev, A.; Tahersima, M. H.; Sorger, V. J.; Naughton, M. J.; Kempa, K.; Dagenais, M.; Yao, Y.; Xu, L.; Sheng, X.; Bronstein, N. D.; Rogers, J. A.; Alivisatos, A. P.; Nuzzo, R. G.; Gordon, J. M.; Wu, D. M.; Wisser, M. D.; Salleo, A.; Dionne, J.; Bermel, P.; Greffet, J.-J.; Celanovic, I.; Soljacic, M.; Manor, A.; Rotschild, C.; Raman, A.; Zhu, L.; Fan, S.; Chen, G. Roadmap on optical energy conversion. *Journal of Optics* **2016**, *18*, 073004.
- (17) Beard, M. C.; Midgett, A. G.; Hanna, M. C.; Luther, J. M.; Hughes, B. K.; Nozik, A. J. Comparing Multiple Exciton Generation in Quantum Dots To Impact Ionization in Bulk Semiconductors: Implications for Enhancement of Solar Energy Conversion. *Nano Lett.* **2010**, *10*, 3019-3027.

- (18) Ellingson, R. J.; Beard, M. C.; Johnson, J. C.; Yu, P.; Micic, O. I.; Nozik, A. J.; Shabaev, A.; Efros, A. L. Highly Efficient Multiple Exciton Generation in Colloidal PbSe and PbS Quantum Dots. *Nano Lett.* **2005**, *5*, 865.
- (19) Nair, G.; Geyer, S. M.; Chang, L. Y.; Bawendi, M. G. Carrier multiplication yields in PbS and PbSe nanocrystals measured by transient photoluminescence. *Phys. Rev. B* **2008**, *78*, 10.
- (20) Trinh, M. T.; Houtepen, A. J.; Schins, J. M.; Hanrath, T.; Piris, J.; Knulst, W.; Goossens, A.; Siebbeles, L. D. A. In spite of recent doubts carrier multiplication does occur in PbSe nanocrystals. *Nano Lett.* **2008**, *8*, 1713-1718.
- (21) Ji, M.; Park, S.; Conner, S. T.; Mokari, T.; Cui, Y.; Gaffney, K. J. Efficient Multiple Exciton Generation Observed in Colloidal PbSe Quantum Dots with Temporally and Spectrally Resolved Intraband Excitation. *Nano Lett.* **2009**, *9*, 1217-1222.
- (22) Stewart, J. T.; Padilha, L. A.; Qazilbash, M. M.; Pietryga, J. M.; Midgett, A. G.; Luther, J. M.; Beard, M. C.; Nozik, A. J.; Klimov, V. I. Comparison of Carrier Multiplication Yields in PbS and PbSe Nanocrystals: The Role of Competing Energy-Loss Processes. *Nano Lett.* **2012**, *12*, 622-628.
- (23) Murphy, J. E.; Beard, M. C.; Norman, A. G.; Ahrenkiel, S. P.; Johnson, J. C.; Yu, P.; Micic, O. I.; Ellingson, R. J.; Nozik, A. J. PbTe Colloidal Nanocrystals: Synthesis, Characterization, and Multiple Exciton Generation. *J. Am. Chem. Soc.* **2006**, *128*, 3241-3247.
- (24) Midgett, A. G.; Smith, D. K.; Luther, J. M.; Stewart, J. T.; Padilha, L. A.; Klimov, V. I.; Nozik, A. J.; Beard, M. C. Size and composition dependent Multiple Exciton Generation Efficiency in PbS, PbSe, and PbS_xSe_{1-x} Alloy Quantum Dots. *Nano Lett.* **2013**, *13*, 3078-3085.
- (25) Stewart, J. T.; Padilha, L. A.; Bae, W. K.; Koh, W. K.; Pietryga, J. M.; Klimov, V. I. Carrier Multiplication in Quantum Dots within the Framework of Two Competing Energy Relaxation Mechanisms. *J. Phys. Chem. Lett.* **2013**, *4*, 2061-2068.
- (26) Luther, J. M.; Beard, M. C.; Song, Q.; Law, M.; Ellingson, R. J.; Nozik, A. J. Multiple exciton generation in films of electronically coupled PbSe quantum dots. *Nano Lett.* **2007**, *7*, 1779-1784.
- (27) Beard, M. C.; Midgett, A. G.; Law, M.; Semonin, O. E.; Ellingson, R. J.; Nozik, A. J. Variations in the Quantum Efficiency of Multiple Exciton Generation for a Series of Chemically Treated PbSe Nanocrystal Films. *Nano Lett.* **2009**, *9*, 836-845.
- (28) ten Cate, S.; Liu, Y.; Sandeep, C. S. S.; Kinge, S.; Houtepen, A. J.; Savenije, T. J.; Schins, J. M.; Law, M.; Siebbeles, L. D. A. Activating Carrier Multiplication in PbSe Quantum Dot Solids by Infilling with Atomic Layer Deposition. *J. Phys. Chem. Lett.* **2013**, *4*, 1766-1770.
- (29) Kulkarni, A.; Evers, W. H.; Tomić, S.; Beard, M. C.; Vanmaekelbergh, D.; Siebbeles, L. D. A. Efficient Step-like Carrier Multiplication in Percolative Networks of Epitaxially Connected PbSe Nanocrystals. *ACS Nano* **2018**, *12*, 378-384.
- (30) Aerts, M.; Sandeep, C. S. S.; Gao, Y. A.; Savenije, T. J.; Schins, J. M.; Houtepen, A. J.; Kinge, S.; Siebbeles, L. D. A. Free Charges Produced by Carrier Multiplication in Strongly Coupled PbSe Quantum Dot Films. *Nano Lett.* **2011**, *11*, 4485-4489.
- (31) Gao, J.; Fidler, A. F.; Klimov, V. I. Carrier multiplication detected through transient photocurrent in device-grade films of lead selenide quantum dots. **2015**, *6*, 8185.
- (32) Beard, M. C.; Knutsen, K. P.; Yu, P. R.; Luther, J. M.; Song, Q.; Metzger, W. K.; Ellingson, R. J.; Nozik, A. J. Multiple exciton generation in colloidal silicon nanocrystals. *Nano Lett.* **2007**, *7*, 2506-2512.
- (33) Timmerman, D.; Izeddin, I.; Stallinga, P.; Yassievich, I. N.; Gregorkiewicz, T. Space-separated quantum cutting with silicon nanocrystals for photovoltaic applications. *Nat. Photonics* **2008**, *2*, 105-109.
- (34) Timmerman, D.; Valenta, J.; Dohnalova, K.; de Boer, W.; Gregorkiewicz, T. Step-like enhancement of luminescence quantum yield of silicon nanocrystals. *Nature Nanotechnology* **2011**, *6*, 710-713.

- (35) Saeed, S.; de Weerd, C.; Stallinga, P.; Spoor, F. C. M.; Houtepen, A. J.; Da Siebbeles, L.; Gregorkiewicz, T. Carrier multiplication in germanium nanocrystals. *Light Sci Appl* **2015**, *4*, e251.
- (36) Schaller, R. D.; Pietryga, J. M.; Klimov, V. I. Carrier Multiplication in InAs Nanocrystal Quantum Dots with an Onset Defined by the Energy Conservation Limit *Nano Lett.* **2007**, *7*, 3469-3476.
- (37) Pijpers, J. J. H.; Hendry, E.; Milder, M. T. W.; Fanciulli, R.; Savolainen, J.; Herek, J. L.; Vanmaekelbergh, D.; Ruhman, S.; Mocatta, D.; Oron, D.; Aharoni, A.; Banin, U.; Bonn, M. Carrier multiplication and its reduction by photodoping in colloidal InAs quantum dots (vol 111, pg 4146, 2007). *J. Phys. Chem. C* **2008**, *112*, 4783-4784.
- (38) Stubbs, S. K.; Hardman, S. J. O.; Graham, D. M.; Spencer, B. F.; Flavell, W. R.; Glarvey, P.; Masala, O.; Pickett, N. L.; Binks, D. J. Efficient carrier multiplication in InP nanoparticles. *Phys. Rev. B* **2010**, *81*.
- (39) Sun, J.; Yu, W.; Usman, A.; Isimjan, T. T.; Dgobbo, S.; Alarousu, E.; Takanahe, K.; Mohammed, O. F. Generation of Multiple Excitons in Ag₂S Quantum Dots: Single High-Energy versus Multiple-Photon Excitation. *The Journal of Physical Chemistry Letters* **2014**, *5*, 659-665.
- (40) Kobayashi, Y.; Udagawa, T.; Tamai, N. Carrier Multiplication in CdTe Quantum Dots by Single-photon Timing Spectroscopy. *Chemistry Letters* **2009**, *38*, 830-831.
- (41) Stolle, C. J.; Schaller, R. D.; Korgel, B. A. Efficient Carrier Multiplication in Colloidal CuInSe₂ Nanocrystals. *The Journal of Physical Chemistry Letters* **2014**, *5*, 3169-3174.
- (42) Li, M.; Begum, R.; Fu, J.; Xu, Q.; Koh, T. M.; Veldhuis, S. A.; Grätzel, M.; Mathews, N.; Mhaisalkar, S.; Sum, T. C. Low threshold and efficient multiple exciton generation in halide perovskite nanocrystals. *Nat Commun* **2018**, *9*, 4197.
- (43) de Weerd, C.; Gomez, L.; Capretti, A.; Lebrun, D. M.; Matsubara, E.; Lin, J.; Ashida, M.; Spoor, F. C. M.; Siebbeles, L. D. A.; Houtepen, A. J.; Suenaga, K.; Fujiwara, Y.; Gregorkiewicz, T. Efficient carrier multiplication in CsPbI₃ perovskite nanocrystals. *Nat Commun* **2018**, *9*, 4199.
- (44) Werner, J. H.; Kolodinski, S.; Queisser, H. J. Novel Optimization Principles and Efficiency Limits for Semiconductor Solar Cells. *Phys. Rev. Lett.* **1994**, *72*, 3851-3854.
- (45) Stolle, C. J.; Lu, X.; Yu, Y.; Schaller, R. D.; Korgel, B. A. Efficient Carrier Multiplication in Colloidal Silicon Nanorods. *Nano Lett.* **2017**, *17*, 5580-5586.
- (46) Cunningham, P. D.; Boercker, J. B.; Foos, E.; Lumb, M. P.; Smith, A. R.; Tischler, J. G.; Melinger, J. S. Enhanced multiple exciton generation in quasi one-dimensional semiconductors. *Nano Lett.* **2011**, DOI: 10.1021/nl202024a.
- (47) Padilha, L. A.; Stewart, J. T.; Sandberg, R. L.; Bae, W. K.; Koh, W. K.; Pietryga, J. M.; Klimov, V. I. Aspect Ratio Dependence of Auger Recombination and Carrier Multiplication in PbSe Nanorods. *Nano Lett.* **2013**, *13*, 1092-1099.
- (48) Aerts, M.; Bielewicz, T.; Klinke, C.; Grozema, F. C.; Houtepen, A. J.; Schins, J. M.; Siebbeles, L. D. A. Highly efficient carrier multiplication in PbS nanosheets. *Nat Commun* **2014**, *5*.
- (49) Kroupa, D. M.; Pach, G. F.; Vörös, M.; Giberti, F.; Chernomordik, B. D.; Crisp, R. W.; Nozik, A. J.; Johnson, J. C.; Singh, R.; Klimov, V. I.; Galli, G.; Beard, M. C. Enhanced Multiple Exciton Generation in PbS|CdS Janus-like Heterostructured Nanocrystals. *ACS Nano* **2018**, *12*, 10084-10094.
- (50) Stewart, J. T.; Padilha, L. A.; Bae, W. K.; Koh, W.-K.; Pietryga, J. M.; Klimov, V. I. Carrier Multiplication in Quantum Dots within the Framework of Two Competing Energy Relaxation Mechanisms. *The Journal of Physical Chemistry Letters* **2013**, *4*, 2061-2068.
- (51) Sukhovatkin, V.; Hinds, S.; Brzozowski, L.; Sargent, E. H. Colloidal Quantum-Dot Photodetectors Exploiting Multiexciton Generation. *Science* **2009**, *324*, 1542-1544.
- (52) Kim, S. J.; Kim, W. J.; Sahoo, Y.; Cartwright, A. N.; Prasad, P. N. Multiple exciton generation and electrical extraction from a PbSe quantum dot photoconductor. *Applied Physics Letters* **2008**, *92*, 3.

- (53) Sambur, J. B.; Novet, T.; Parkinson, B. A. Multiple Exciton Collection in a Sensitized Photovoltaic System. *Science* **2010**, *330*, 63-66.
- (54) Semonin, O. E.; Luther, J. M.; Choi, S.; Chen, H.-Y.; Gao, J.; Nozik, A. J.; Beard, M. C. Peak External Photocurrent Quantum Efficiency Exceeding 100% via MEG in a Quantum Dot Solar Cell. *Science* **2011**, *334*, 1530-1533.
- (55) Davis, N. J. L. K.; Bohm, M. L.; Tabachnyk, M.; Wisnivesky-Rocca-Rivarola, F.; Jellicoe, T. C.; Ducati, C.; Ehrler, B.; Greenham, N. C. Multiple-exciton generation in lead selenide nanorod solar cells with external quantum efficiencies exceeding 120%. *Nat Commun* **2015**, *6*, 8259.
- (56) Böhm, M. L.; Jellicoe, T. C.; Tabachnyk, M.; Davis, N. J. L. K.; Wisnivesky-Rocca-Rivarola, F.; Ducati, C.; Ehrler, B.; Bakulin, A. A.; Greenham, N. C. Lead Telluride Quantum Dot Solar Cells Displaying External Quantum Efficiencies Exceeding 120%. *Nano Lett.* **2015**, *15*, 7987-7993.
- (57) Ellingson, R. J.; Beard, M. C.; Johnson, J. C.; Yu, P.; Micic, O. I.; Nozik, A. J.; Shabaev, A.; Efros, A. L. Highly Efficient Multiple Exciton Generation in Colloidal PbSe and PbS Quantum Dots. *Nano Letters* **2005**, *5*, 865-871.
- (58) Schaller, R. D.; Sykora, M.; Jeong, S.; Klimov, V. I. High-Efficiency Carrier Multiplication and Ultrafast Charge Separation in Semiconductor Nanocrystals Studied via Time-Resolved Photoluminescence. *The Journal of Physical Chemistry B* **2006**, *110*, 25332-25338.
- (59) Beard, M. C.; Ellingson, R. J. Multiple exciton generation in semiconductor nanocrystals: Toward efficient solar energy conversion. *Laser & Photonics Reviews* **2008**, *2*, 377-399.
- (60) Nair, G.; Geyer, S. M.; Chang, L.-Y.; Bawendi, M. G. Carrier multiplication yields in PbS and PbSe nanocrystals measured by transient photoluminescence. *Physical Review B* **2008**, *78*, 125325.
- (61) Pijpers, J. J. H.; Hendry, E.; Milder, M. T. W.; Fanciulli, R.; Savolainen, J.; Herek, J. L.; Vanmaekelbergh, D.; Ruhman, S.; Mocatta, D.; Oron, D.; Aharoni, A.; Banin, U.; Bonn, M. Carrier Multiplication and Its Reduction by Photodoping in Colloidal InAs Quantum Dots. *The Journal of Physical Chemistry C* **2008**, *112*, 4783-4784.
- (62) Ben-Lulu, M.; Mocatta, D.; Bonn, M.; Banin, U.; Ruhman, S. On the Absence of Detectable Carrier Multiplication in a Transient Absorption Study of InAs/CdSe/ZnSe Core/Shell1/Shell2 Quantum Dots. *Nano Letters* **2008**, *8*, 1207-1211.
- (63) Beard, M. C. Multiple Exciton Generation in Semiconductor Quantum Dots. *The Journal of Physical Chemistry Letters* **2011**, *2*, 1282-1288.
- (64) Winzer, T.; Knorr, A.; Malic, E. Carrier Multiplication in Graphene. *Nano Letters* **2010**, *10*, 4839-4843.
- (65) McGuire, J. A.; Sykora, M.; Joo, J.; Pietryga, J. M.; Klimov, V. I. Apparent Versus True Carrier Multiplication Yields in Semiconductor Nanocrystals. *Nano Letters* **2010**, *10*, 2049-2057.
- (66) McGuire, J. A.; Joo, J.; Pietryga, J. M.; Schaller, R. D.; Klimov, V. I. New Aspects of Carrier Multiplication in Semiconductor Nanocrystals. *Accounts of Chemical Research* **2008**, *41*, 1810-1819.
- (67) Midgett, A. G.; Hillhouse, H. W.; Hughes, B. K.; Nozik, A. J.; Beard, M. C. Flowing versus Static Conditions for Measuring Multiple Exciton Generation in PbSe Quantum Dots. *The Journal of Physical Chemistry C* **2010**, *114*, 17486-17500.
- (68) McDaniel, H.; Fuke, N.; Pietryga, J. M.; Klimov, V. I. Engineered CuInSexS2-x Quantum Dots for Sensitized Solar Cells. *The Journal of Physical Chemistry Letters* **2013**, *4*, 355-361.
- (69) Lai, L.-H.; Protesescu, L.; V. Kovalenko, M.; A. Loi, M. Sensitized solar cells with colloidal PbS-CdS core-shell quantum dots. *Physical Chemistry Chemical Physics* **2014**, *16*, 736-742.
- (70) Kamat, P. V. Quantum Dot Solar Cells. Semiconductor Nanocrystals as Light Harvesters. *The Journal of Physical Chemistry C* **2008**, *112*, 18737-18753.
- (71) Piliago, C.; Manca, M.; Kroon, R.; Yarema, M.; Szendrei, K.; R. Andersson, M.; Heiss, W.; A. Loi, M. Charge separation dynamics in a narrow band gap polymer -PbS nanocrystal blend for efficient hybrid solar cells. *Journal of Materials Chemistry* **2012**, *22*, 24411-24416.

- (72) Huynh, W. U.; Dittmer, J. J.; Alivisatos, A. P. Hybrid Nanorod-Polymer Solar Cells. *Science* **2002**, *295*, 2425.
- (73) Lu, H.; Joy, J.; Gaspar, R. L.; Bradforth, S. E.; Brutchey, R. L. Iodide-Passivated Colloidal PbS Nanocrystals Leading to Highly Efficient Polymer:Nanocrystal Hybrid Solar Cells. *Chemistry of Materials* **2016**, *28*, 1897-1906.
- (74) Lu, H.; Brutchey, R. L.: Hybrid Polymer: Nanocrystal Solar Cells. In *World Scientific Handbook of Organic Optoelectronic Devices; Materials and Energy*; World Scientific, 2018; pp 405-444.
- (75) Luther, J. M.; Law, M.; Beard, M. C.; Song, Q.; Reese, M. O.; Ellingson, R. J.; Nozik, A. J. Schottky Solar Cells Based on Colloidal Nanocrystal Films. *Nano Letters* **2008**, *8*, 3488-3492.
- (76) Johnston, K. W.; Pattantyus-Abraham, A. G.; Clifford, J. P.; Myrskog, S. H.; MacNeil, D. D.; Levina, L.; Sargent, E. H. Schottky-quantum dot photovoltaics for efficient infrared power conversion. *Applied Physics Letters* **2008**, *92*, 151115.
- (77) Ma, W.; Luther, J. M.; Zheng, H.; Wu, Y.; Alivisatos, A. P. Photovoltaic Devices Employing Ternary PbS_xSe_{1-x} Nanocrystals. *Nano Lett.* **2009**, *9*, 5.
- (78) Luther, J. M.; Gao, J.; Lloyd, M. T.; Semonin, O. E.; Beard, M. C.; Nozik, A. J. Stability Assessment on a 3% Bilayer PbS/ZnO Quantum Dot Heterojunction Solar Cell. *Advanced Materials* **2010**, *22*, 3704-3707.
- (79) Baek, S.-W.; Jun, S.; Kim, B.; Proppe, A. H.; Ouellette, O.; Voznyy, O.; Kim, C.; Kim, J.; Walters, G.; Song, J. H.; Jeong, S.; Byun, H. R.; Jeong, M. S.; Hoogland, S.; García de Arquer, F. P.; Kelley, S. O.; Lee, J.-Y.; Sargent, E. H. Efficient hybrid colloidal quantum dot/organic solar cells mediated by near-infrared sensitizing small molecules. *Nature Energy* **2019**, *4*, 969-976.
- (80) Zhao, Q.; Hazarika, A.; Chen, X.; Harvey, S. P.; Larson, B. W.; Teeter, G. R.; Liu, J.; Song, T.; Xiao, C.; Shaw, L.; Zhang, M.; Li, G.; Beard, M. C.; Luther, J. M. High efficiency perovskite quantum dot solar cells with charge separating heterostructure. *Nature Communications* **2019**, *10*, 2842.
- (81) Hao, M.; Bai, Y.; Zeiske, S.; Ren, L.; Liu, J.; Yuan, Y.; Zarrabi, N.; Cheng, N.; Ghasemi, M.; Chen, P.; Lyu, M.; He, D.; Yun, J.-H.; Du, Y.; Wang, Y.; Ding, S.; Armin, A.; Meredith, P.; Liu, G.; Cheng, H.-M.; Wang, L. Ligand-assisted cation-exchange engineering for high-efficiency colloidal Cs_{1-x}FaxPbI₃ quantum dot solar cells with reduced phase segregation. *Nature Energy* **2020**, *5*, 79-88.
- (82) Chuang, C.-H. M.; Brown, P. R.; Bulović, V.; Bawendi, M. G. Improved performance and stability in quantum dot solar cells through band alignment engineering. *Nature Materials* **2014**, *13*, 796-801.
- (83) Chernomordik, B. D.; Marshall, A. R.; Pach, G. F.; Luther, J. M.; Beard, M. C. Quantum Dot Solar Cell Fabrication Protocols. *Chemistry of Materials* **2017**, *29*, 189-198.
- (84) Crisp, R. W.; Kroupa, D. M.; Marshall, A. R.; Miller, E. M.; Zhang, J.; Beard, M. C.; Luther, J. M. Metal Halide Solid-State Surface Treatment for High Efficiency PbS and PbSe QD Solar Cells. *Scientific Reports* **2015**, *5*, 9945.
- (85) Chuang, C.-H. M.; Maurano, A.; Brandt, R. E.; Hwang, G. W.; Jean, J.; Buonassisi, T.; Bulović, V.; Bawendi, M. G. Open-Circuit Voltage Deficit, Radiative Sub-Bandgap States, and Prospects in Quantum Dot Solar Cells. *Nano Letters* **2015**, *15*, 3286-3294.
- (86) Ip, A. H.; Thon, S. M.; Hoogland, S.; Voznyy, O.; Zhitomirsky, D.; Debnath, R.; Levina, L.; Rollny, L. R.; Carey, G. H.; Fischer, A.; Kemp, K. W.; Kramer, I. J.; Ning, Z.; Labelle, A. J.; Chou, K. W.; Amassian, A.; Sargent, E. H. Hybrid passivated colloidal quantum dot solids. *Nature Nanotechnology* **2012**, *7*, 577-582.
- (87) Kroupa, D. M.; Vörös, M.; Brawand, N. P.; Bronstein, N.; McNichols, B. W.; Castaneda, C. V.; Nozik, A. J.; Sellinger, A.; Galli, G.; Beard, M. C. Optical Absorbance Enhancement in PbS QD/Cinnamate Ligand Complexes. *The Journal of Physical Chemistry Letters* **2018**, *9*, 3425-3433.

- (88) Giansante, C.; Infante, I.; Fabiano, E.; Grisorio, R.; Suranna, G. P.; Gigli, G. "Darker-than-Black" PbS Quantum Dots: Enhancing Optical Absorption of Colloidal Semiconductor Nanocrystals via Short Conjugated Ligands. *Journal of the American Chemical Society* **2015**, *137*, 1875-1886.
- (89) Frederick, M. T.; Weiss, E. A. Relaxation of Exciton Confinement in CdSe Quantum Dots by Modification with a Conjugated Dithiocarbamate Ligand. *ACS Nano* **2010**, *4*, 3195-3200.
- (90) Luther, J. M.; Law, M.; Song, Q.; Perkins, C. L.; Beard, M. C.; Nozik, A. J. Structural, Optical, and Electrical Properties of Self-Assembled Films of PbSe Nanocrystals Treated with 1,2-Ethanedithiol. *ACS Nano* **2008**, *2*, 271-280.
- (91) Yu, D.; Wang, C.; Guyot-Sionnest, P. n-Type Conducting CdSe Nanocrystal Solids. *Science* **2003**, *300*, 1277-1280.
- (92) Lu, H.; Carroll, G. M.; Chen, X.; Amarasinghe, D. K.; Neale, N. R.; Miller, E. M.; Sercel, P. C.; Rabuffetti, F. A.; Efros, A. L.; Beard, M. C. n-Type PbSe Quantum Dots via Post-Synthetic Indium Doping. *Journal of the American Chemical Society* **2018**, *140*, 13753-13763.
- (93) Guglietta, G. W.; Diroll, B. T.; Gauding, E. A.; Fordham, J. L.; Li, S.; Murray, C. B.; Baxter, J. B. Lifetime, Mobility, and Diffusion of Photoexcited Carriers in Ligand-Exchanged Lead Selenide Nanocrystal Films Measured by Time-Resolved Terahertz Spectroscopy. *ACS Nano* **2015**, *9*, 1820-1828.
- (94) Semonin, O. E.; Luther, J. M.; Choi, S.; Chen, H. Y.; Gao, J. B.; Nozik, A. J.; Beard, M. C. Peak External Photocurrent Quantum Efficiency Exceeding 100% via MEG in a Quantum Dot Solar Cell. *Science* **2011**, *334*, 1530-1533.
- (95) Xu, J.; Voznyy, O.; Liu, M.; Kirmani, A. R.; Walters, G.; Munir, R.; Abdelsamie, M.; Proppe, A. H.; Sarkar, A.; García de Arquer, F. P.; Wei, M.; Sun, B.; Liu, M.; Ouellette, O.; Quintero-Bermudez, R.; Li, J.; Fan, J.; Quan, L.; Todorovic, P.; Tan, H.; Hoogland, S.; Kelley, S. O.; Stefik, M.; Amassian, A.; Sargent, E. H. 2D matrix engineering for homogeneous quantum dot coupling in photovoltaic solids. *Nature Nanotechnology* **2018**, *13*, 456-462.
- (96) Ouellette, O.; Lesage-Landry, A.; Scheffel, B.; Hoogland, S.; García de Arquer, F. P.; Sargent, E. H. Spatial Collection in Colloidal Quantum Dot Solar Cells. *Advanced Functional Materials* **2019**, *n/a*, 1908200.
- (97) Crisp, R. W.; D., K.; Marshall, A.; Zhang, J.; Beard, M. C.; Luther, J. M. Metal Halide Solid-State Surface Treatment for High Efficiency PbS and PbSe QD Solar Cells. *Sci Rep* **2015**, *5*, 9945.
- (98) Sargent, E. H. - Infrared photovoltaics made by solution processing. **2009**, - 3, - 331.
- (99) Choi, J. J.; Wenger, W. N.; Hoffman, R. S.; Lim, Y.-F.; Luria, J.; Jasieniak, J.; Marohn, J. A.; Hanrath, T. Solution-Processed Nanocrystal Quantum Dot Tandem Solar Cells. *Adv. Mater.* **2011**, *23*, 3144 - 3148.
- (100) Wang, X.; Koleilat, G. I.; Tang, J.; Liu, H.; Kramer, I. J.; Debnath, R.; Brzozowski, L.; Barkhouse, D. A. R.; Levina, L.; Hoogland, S.; Sargent, E. H. Tandem colloidal quantum dot solar cells employing a graded recombination layer. *Nat. Photonics* **2011**, *5*, 480 - 484.
- (101) Crisp, R. W.; Pach, G. F.; Kurley, J. M.; France, R. M.; Reese, M. O.; Nanayakkara, S. U.; MacLeod, B. A.; Talapin, D. V.; Beard, M. C.; Luther, J. M. Tandem Solar Cells from Solution-Processed CdTe and PbS Quantum Dots Using a ZnTe-ZnO Tunnel Junction. *Nano Letters* **2017**, *17*, 1020-1027.
- (102) Protesescu, L.; Yakunin, S.; Bodnarchuk, M. I.; Krieg, F.; Caputo, R.; Hendon, C. H.; Yang, R. X.; Walsh, A.; Kovalenko, M. V. Nanocrystals of Cesium Lead Halide Perovskites (CsPbX₃, X = Cl, Br, and I): Novel Optoelectronic Materials Showing Bright Emission with Wide Color Gamut. *Nano Letters* **2015**, *15*, 3692-3696.
- (103) Li, Z.; Yang, M.; Park, J.-S.; Wei, S.-H.; Berry, J. J.; Zhu, K. Stabilizing Perovskite Structures by Tuning Tolerance Factor: Formation of Formamidinium and Cesium Lead Iodide Solid-State Alloys. *Chemistry of Materials* **2016**, *28*, 284-292.

- (104) Zhao, Q.; Hazarika, A.; Schelhas, L. T.; Liu, J.; Gaubing, E. A.; Li, G.; Zhang, M.; Toney, M. F.; Sercel, P. C.; Luther, J. M. Size-Dependent Lattice Structure and Confinement Properties in CsPbI₃ Perovskite Nanocrystals: Negative Surface Energy for Stabilization. *ACS Energy Lett.* **2020**, *5*, 238-247.
- (105) Swarnkar, A.; Marshall, A. R.; Sanehira, E. M.; Chernomordik, B. D.; Moore, D. T.; Christians, J. A.; Chakrabarti, T.; Luther, J. M. Quantum dot-induced phase stabilization of α -CsPbI₃ perovskite for high-efficiency photovoltaics. *Science* **2016**, *354*, 92-95.
- (106) Sanehira, E. M.; Marshall, A. R.; Christians, J. A.; Harvey, S. P.; Ciesielski, P. N.; Wheeler, L. M.; Schulz, P.; Lin, L. Y.; Beard, M. C.; Luther, J. M. Enhanced mobility CsPbI₃ quantum dot arrays for record-efficiency, high-voltage photovoltaic cells. *SCIENCE ADVANCES* **2017**, *9*.
- (107) Hazarika, A.; Zhao, Q.; Gaubing, E. A.; Christians, J. A.; Dou, B.; Marshall, A. R.; Moot, T.; Berry, J. J.; Johnson, J. C.; Luther, J. M. Perovskite Quantum Dot Photovoltaic Materials beyond the Reach of Thin Films: Full-Range Tuning of A-Site Cation Composition. *ACS Nano* **2018**, *12*, 10327-10337.
- (108) Yuan, J.; Ling, X.; Yang, D.; Li, F.; Zhou, S.; Shi, J.; Qian, Y.; Hu, J.; Sun, Y.; Yang, Y.; Gao, X.; Duhm, S.; Zhang, Q.; Ma, W. Band-Aligned Polymeric Hole Transport Materials for Extremely Low Energy Loss α -CsPbI₃ Perovskite Nanocrystal Solar Cells. *Joule* **2018**, *2*, 2450-2463.
- (109) Suri, M.; Hazarika, A.; Larson, B. W.; Zhao, Q.; Vallés-Pelarda, M.; Siegler, T. D.; Abney, M. K.; Ferguson, A. J.; Korgel, B. A.; Luther, J. M. Enhanced Open-Circuit Voltage of Wide-Bandgap Perovskite Photovoltaics by Using Alloyed (FA_{1-x}Cs_x)Pb(I_{1-x}Br_x)₃ Quantum Dots. *ACS Energy Lett.* **2019**, *4*, 1954-1960.
- (110) Schulze, T. F.; Schmidt, T. W. Photochemical upconversion: present status and prospects for its application to solar energy conversion. *Energy Environ. Sci.* **2015**, *8*, 103-125.
- (111) Smith, M. B.; Michl, J. Singlet Fission. *Chem. Rev.* **2010**, *110*, 6891-6936.
- (112) Zhou, J.; Liu, Q.; Feng, W.; Sun, Y.; Li, F. Upconversion luminescent materials: advances and applications. *Chem. Rev.* **2014**, *115*, 395-465.
- (113) Chen, G.; Qiu, H.; Prasad, P. N.; Chen, X. Upconversion nanoparticles: design, nanochemistry, and applications in theranostics. *Chem. Rev.* **2014**, *114*, 5161-5214.
- (114) Singh-Rachford, T. N.; Castellano, F. N. Photon upconversion based on sensitized triplet-triplet annihilation. *Coordination Chemistry Reviews* **2010**, *254*, 2560-2573.
- (115) Huang, Z.; Lee Tang, M. Semiconductor Nanocrystal Light Absorbers for Photon Upconversion. *The Journal of Physical Chemistry Letters* **2018**, *9*, 6198-6206.
- (116) Khnayzer, R. S.; Blumhoff, J.; Harrington, J. A.; Haefele, A.; Deng, F.; Castellano, F. N. Upconversion-powered photoelectrochemistry. *Chemical Communications* **2012**, *48*, 209-211.
- (117) Huang, Z.; Li, X.; Mahboub, M.; Hanson, K. M.; Nichols, V. M.; Le, H.; Tang, M. L.; Bardeen, C. J. Hybrid molecule-nanocrystal photon upconversion across the visible and near-infrared. *Nano Lett.* **2015**, *15*, 5552-5557.
- (118) Wu, M.; Congreve, D. N.; Wilson, M. W.; Jean, J.; Geva, N.; Welborn, M.; Van Voorhis, T.; Bulović, V.; Bawendi, M. G.; Baldo, M. A. Solid-state infrared-to-visible upconversion sensitized by colloidal nanocrystals. *Nat. Photonics* **2016**, *10*, 31-34.
- (119) Huang, Z.; Tang, M. L. Designing Transmitter Ligands That Mediate Energy Transfer between Semiconductor Nanocrystals and Molecules. *J Am Chem Soc* **2017**, *139*, 9412-9418.
- (120) Li, X.; Huang, Z.; Zavala, R.; Tang, M. L. Distance-Dependent Triplet Energy Transfer between CdSe Nanocrystals and Surface Bound Anthracene. *The Journal of Physical Chemistry Letters* **2016**, *7*, 1955-1959.
- (121) Huang, Z.; Simpson, D. E.; Mahboub, M.; Li, X.; Tang, M. L. Ligand enhanced upconversion of near-infrared photons with nanocrystal light absorbers. *Chemical Science* **2016**.
- (122) Mongin, C.; Garakyaraghi, S.; Razgoniaeva, N.; Zamkov, M.; Castellano, F. N. Direct observation of triplet energy transfer from semiconductor nanocrystals. *Science* **2016**, *351*, 369-372.

- (123) Nienhaus, L.; Wu, M.; Geva, N.; Shepherd, J. J.; Wilson, M. W.; Bulović, V.; Van Voorhis, T.; Baldo, M. A.; Bawendi, M. G. Speed Limit for Triplet-Exciton Transfer in Solid-State PbS Nanocrystal-Sensitized Photon Upconversion. *ACS Nano* **2017**.
- (124) Huang, Z.; Li, X.; Yip, B. D.; Rubalcava, J. M.; Bardeen, C. J.; Tang, M. L. Nanocrystal Size and Quantum Yield in the Upconversion of Green to Violet Light with CdSe and Anthracene Derivatives. *Chemistry of Materials* **2015**, *27*, 7503-7507.
- (125) Mahboub, M.; Maghsoudiganjeh, H.; Pham, A. M.; Huang, Z.; Tang, M. L. Triplet Energy Transfer from PbS (Se) Nanocrystals to Rubrene: the Relationship between the Upconversion Quantum Yield and Size. *Adv Funct Mater* **2016**.
- (126) Okumura, K.; Mase, K.; Yanai, N.; Kimizuka, N. Employing Core-Shell Quantum Dots as Triplet Sensitizers for Photon Upconversion. *Chemistry – A European Journal* **2016**, *22*, 7721-7726.
- (127) Mahboub, M.; Huang, Z.; Tang, M. L. Efficient Infrared-to-Visible Upconversion with Subsolar Irradiance. *Nano Lett.* **2016**, *16*, 7169-7175.
- (128) Gray, V.; Xia, P.; Huang, Z.; Moses, E.; Fast, A.; Fishman, D. A.; Vullev, V. I.; Abrahamsson, M.; Moth-Poulsen, K.; Lee Tang, M. CdS/ZnS core-shell nanocrystal photosensitizers for visible to UV upconversion. *Chemical Science* **2017**.
- (129) Huang, Z.; Xu, Z.; Mahboub, M.; Li, X.; Taylor, J. W.; Harman, W. H.; Lian, T.; Tang, M. L. PbS/CdS Core-Shell Quantum Dots Suppress Charge Transfer and Enhance Triplet Transfer. *Angewandte Chemie International Edition* **2017**, *56*, 16583-16587.
- (130) Bender, J. A.; Raulerson, E. K.; Li, X.; Goldzak, T.; Xia, P.; Van Voorhis, T.; Tang, M. L.; Roberts, S. T. Surface States Mediate Triplet Energy Transfer in Nanocrystal-Acene Composite Systems. *J Am Chem Soc* **2018**.
- (131) Han, Y.; He, S.; Luo, X.; Li, Y.; Chen, Z.; Kang, W.; Wang, X.; Wu, K. Triplet Sensitization by "Self-Trapped" Excitons of Nontoxic CuInS₂ Nanocrystals for Efficient Photon Upconversion. *J Am Chem Soc* **2019**, *141*, 13033-13037.
- (132) Mase, K.; Okumura, K.; Yanai, N.; Kimizuka, N. Triplet sensitization by perovskite nanocrystals for photon upconversion. *Chemical Communications* **2017**, *53*, 8261-8264.
- (133) Luo, X.; Lai, R.; Li, Y.; Han, Y.; Liang, G.; Liu, X.; Ding, T.; Wang, J.; Wu, K. Triplet Energy Transfer from CsPbBr₃ Nanocrystals Enabled by Quantum Confinement. *Journal of the American Chemical Society* **2019**, *141*, 4186-4190.
- (134) He, S.; Luo, X.; Liu, X.; Li, Y.; Wu, K. Visible-to-Ultraviolet Upconversion Efficiency above 10% Sensitized by Quantum-Confined Perovskite Nanocrystals. *The Journal of Physical Chemistry Letters* **2019**, *10*, 5036-5040.
- (135) Congreve, D. N.; Lee, J.; Thompson, N. J.; Hontz, E.; Yost, S. R.; Reuswig, P. D.; Bahlke, M. E.; Reineke, S.; Van Voorhis, T.; Baldo, M. A. External Quantum Efficiency Above 100% in a Singlet-Exciton-Fission-Based Organic Photovoltaic Cell. *Science* **2013**, *340*, 334-337.
- (136) Futscher, M. H.; Rao, A.; Ehrler, B. The Potential of Singlet Fission Photon Multipliers as an Alternative to Silicon-Based Tandem Solar Cells. *ACS Energy Letters* **2018**, *3*, 2587-2592.
- (137) Baldo, M. A.; O'Brien, D. F.; You, Y.; Shoustikov, A.; Sibley, S.; Thompson, M. E.; Forrest, S. R. Highly efficient phosphorescent emission from organic electroluminescent devices. *Nature* **1998**, *395*, 151-154.
- (138) Semonin, O. E.; Johnson, J. C.; Luther, J. M.; Midgett, A. G.; Nozik, A. J.; Beard, M. C. Absolute Photoluminescence Quantum Yields of IR-26 Dye, PbS, and PbSe Quantum Dots. *The Journal of Physical Chemistry Letters* **2010**, *1*, 2445-2450.
- (139) Engman, R.; Jortner, J. The energy gap law for radiationless transitions in large molecules. *Molecular Physics* **1970**, *18*, 145-164.
- (140) Nirmal, M.; Norris, D. J.; Kuno, M.; Bawendi, M. G.; Efros, A. L.; Rosen, M. Observation of the "Dark Exciton" in CdSe Quantum Dots. *Physical Review Letters* **1995**, *75*, 3728-3731.

- (141) Thompson, N. J.; Wilson, M. W. B.; Congreve, D. N.; Brown, P. R.; Scherer, J. M.; Bischof, Thomas S.; Wu, M.; Geva, N.; Welborn, M.; Voorhis, T. V.; Bulović, V.; Bawendi, M. G.; Baldo, Marc A. Energy harvesting of non-emissive triplet excitons in tetracene by emissive PbS nanocrystals. *Nat Mater* **2014**, *13*, 1039-1043.
- (142) Tabachnyk, M.; Ehrler, B.; Gélinas, S.; Böhm, M. L.; Walker, B. J.; Musselman, K. P.; Greenham, N. C.; Friend, R. H.; Rao, A. Resonant energy transfer of triplet excitons from pentacene to PbSe nanocrystals. *Nat. Mater.* **2014**, *13*, 1033-1038.
- (143) Davis, N. J. L. K.; Allardice, J. R.; Xiao, J.; Petty, A. J.; Greenham, N. C.; Anthony, J. E.; Rao, A. Singlet Fission and Triplet Transfer to PbS Quantum Dots in TIPS-Tetracene Carboxylic Acid Ligands. *The Journal of Physical Chemistry Letters* **2018**, *9*, 1454-1460.
- (144) Allardice, J. R.; Thampi, A.; Dowland, S.; Xiao, J.; Gray, V.; Zhang, Z.; Budden, P.; Petty, A. J.; Davis, N. J. L. K.; Greenham, N. C.; Anthony, J. E.; Rao, A. Engineering Molecular Ligand Shells on Quantum Dots for Quantitative Harvesting of Triplet Excitons Generated by Singlet Fission. *J Am Chem Soc* **2019**, *141*, 12907-12915.
- (145) Einzinger, M.; Wu, T.; Kompalla, J. F.; Smith, H. L.; Perkinson, C. F.; Nienhaus, L.; Wieghold, S.; Congreve, D. N.; Kahn, A.; Bawendi, M. G.; Baldo, M. A. Sensitization of silicon by singlet exciton fission in tetracene. *Nature* **2019**, *571*, 90-94.
- (146) Lu, H.; Chen, X.; Anthony, J. E.; Johnson, J. C.; Beard, M. C. Sensitizing Singlet Fission with Perovskite Nanocrystals. *J Am Chem Soc* **2019**, *141*, 4919-4927.
- (147) Wegh, R. T.; Donker, H.; Oskam, K. D.; Meijerink, A. Visible Quantum Cutting in $\text{LiGdF}_4:\text{Eu}^{3+}$ Through Downconversion. *Science* **1999**, *283*, 663-666.
- (148) Srivastava, A. M.; Doughty, D. A.; Beers, W. W. Photon Cascade Luminescence of Pr^{3+} in $\text{LaMgB}_5\text{O}_{10}$. *Journal of The Electrochemical Society* **1996**, *143*, 4113-4116.
- (149) Pappalardo, R. Calculated quantum yields for photon-cascade emission (PCE) for Pr^{3+} and Tm^{3+} in fluoride hosts. *Journal of Luminescence* **1976**, *14*, 159-193.
- (150) Sommerdijk, J. L.; Bril, A.; de Jager, A. W. Two photon luminescence with ultraviolet excitation of trivalent praseodymium. *Journal of Luminescence* **1974**, *8*, 341-343.
- (151) Milstein, T. J.; Kluherz, K. T.; Kroupa, D. M.; Erickson, C. S.; De Yoreo, J. J.; Gamelin, D. R. Anion Exchange and the Quantum-Cutting Energy Threshold in Ytterbium-Doped $\text{CsPb}(\text{Cl}_{1-x}\text{Br}_x)_3$ Perovskite Nanocrystals. *Nano Lett.* **2019**, *19*, 1931-1937.
- (152) Crane, M. J.; Kroupa, D. M.; Gamelin, D. R. Detailed-balance analysis of $\text{Yb}^{3+}:\text{CsPb}(\text{Cl}_{1-x}\text{Br}_x)_3$ quantum-cutting layers for high-efficiency photovoltaics under real-world conditions. *Energy Environ. Sci.* **2019**, *12*, 2486-2495.
- (153) Cohen, T. A.; Milstein, T. J.; Kroupa, D. M.; MacKenzie, J. D.; Luscombe, C. K.; Gamelin, D. R. Quantum-cutting Yb^{3+} -doped perovskite nanocrystals for monolithic bilayer luminescent solar concentrators. *J. Mater. Chem. A* **2019**, *7*, 9279-9288.
- (154) Zhou, D.; Liu, D.; Pan, G.; Chen, X.; Li, D.; Xu, W.; Bai, X.; Song, H. Cerium and Ytterbium Codoped Halide Perovskite Quantum Dots: A Novel and Efficient Downconverter for Improving the Performance of Silicon Solar Cells. *Advanced Materials* **2017**, *29*, 1704149.
- (155) Li, X.-B.; Tung, C.-H.; Wu, L.-Z. Quantum Dot Assembly for Light-Driven Multielectron Redox Reactions, such as Hydrogen Evolution and CO_2 Reduction. *Angewandte Chemie International Edition* **2019**, *58*, 10804-10811.
- (156) Waiskopf, N.; Ben-Shahar, Y.; Banin, U. Photocatalytic Hybrid Semiconductor–Metal Nanoparticles; from Synergistic Properties to Emerging Applications. *Advanced Materials* **2018**, *30*, 1706697.
- (157) Han, Z.; Qiu, F.; Eisenberg, R.; Holland, P. L.; Krauss, T. D. Robust Photogeneration of H_2 in Water Using Semiconductor Nanocrystals and a Nickel Catalyst. *Science* **2012**, *338*, 1321.

- (158) Brown, K. A.; Wilker, M. B.; Boehm, M.; Dukovic, G.; King, P. W. Characterization of Photochemical Processes for H₂ Production by CdS Nanorod–[FeFe] Hydrogenase Complexes. *Journal of the American Chemical Society* **2012**, *134*, 5627-5636.
- (159) Yan, Y.; Crisp, R. W.; Gu, J.; Chernomordik, B. D.; Pach, G. F.; Marshall, Ashley R.; Turner, J. A.; Beard, M. C. Multiple exciton generation for photoelectrochemical hydrogen evolution reactions with quantum yields exceeding 100%. *Nature Energy* **2017**, *2*, 17052.
- (160) Chen, X.; Shen, S.; Guo, L.; Mao, S. S. Semiconductor-based Photocatalytic Hydrogen Generation. *Chemical Reviews* **2010**, *110*, 6503-6570.
- (161) Bao, N.; Shen, L.; Takata, T.; Domen, K. Self-Templated Synthesis of Nanoporous CdS Nanostructures for Highly Efficient Photocatalytic Hydrogen Production under Visible Light. *Chemistry of Materials* **2008**, *20*, 110-117.
- (162) Reber, J. F.; Rusek, M. Photochemical hydrogen production with platinized suspensions of cadmium sulfide and cadmium zinc sulfide modified by silver sulfide. *The Journal of Physical Chemistry* **1986**, *90*, 824-834.
- (163) Peng, X.; Manna, L.; Yang, W.; Wickham, J.; Scher, E.; Kadavanich, A.; Alivisatos, A. P. Shape control of CdSe nanocrystals. *Nature* **2000**, *404*, 59-61.
- (164) Li, L.-s.; Hu, J.; Yang, W.; Alivisatos, A. P. Band Gap Variation of Size- and Shape-Controlled Colloidal CdSe Quantum Rods. *Nano Letters* **2001**, *1*, 349-351.
- (165) Mokari, T.; Rothenberg, E.; Popov, I.; Costi, R.; Banin, U. Selective Growth of Metal Tips onto Semiconductor Quantum Rods and Tetrapods. *Science* **2004**, *304*, 1787.
- (166) Wu, K.; Lian, T. Quantum confined colloidal nanorod heterostructures for solar-to-fuel conversion. *Chemical Society Reviews* **2016**, *45*, 3781-3810.
- (167) Amirav, L.; Alivisatos, A. P. Photocatalytic Hydrogen Production with Tunable Nanorod Heterostructures. *The Journal of Physical Chemistry Letters* **2010**, *1*, 1051-1054.
- (168) Nakibli, Y.; Kalisman, P.; Amirav, L. Less Is More: The Case of Metal Cocatalysts. *The Journal of Physical Chemistry Letters* **2015**, *6*, 2265-2268.
- (169) Schweinberger, F. F.; Berr, M. J.; Döblinger, M.; Wolff, C.; Sanwald, K. E.; Crampton, A. S.; Ridge, C. J.; Jäckel, F.; Feldmann, J.; Tschurl, M.; Heiz, U. Cluster Size Effects in the Photocatalytic Hydrogen Evolution Reaction. *Journal of the American Chemical Society* **2013**, *135*, 13262-13265.
- (170) Ben-Shahar, Y.; Scotognella, F.; Kriegel, I.; Moretti, L.; Cerullo, G.; Rabani, E.; Banin, U. Optimal metal domain size for photocatalysis with hybrid semiconductor-metal nanorods. *Nature Communications* **2016**, *7*, 10413.
- (171) Kalisman, P.; Nakibli, Y.; Amirav, L. Perfect Photon-to-Hydrogen Conversion Efficiency. *Nano Letters* **2016**, *16*, 1776-1781.
- (172) Zhu, H.; Song, N.; Lv, H.; Hill, C. L.; Lian, T. Near Unity Quantum Yield of Light-Driven Redox Mediator Reduction and Efficient H₂ Generation Using Colloidal Nanorod Heterostructures. *Journal of the American Chemical Society* **2012**, *134*, 11701-11708.
- (173) Acharya, K. P.; Khnayzer, R. S.; O'Connor, T.; Diederich, G.; Kirsanova, M.; Klinkova, A.; Roth, D.; Kinder, E.; Imboden, M.; Zamkov, M. The Role of Hole Localization in Sacrificial Hydrogen Production by Semiconductor–Metal Heterostructured Nanocrystals. *Nano Letters* **2011**, *11*, 2919-2926.
- (174) Khon, E.; Lambright, K.; Khnayzer, R. S.; Moroz, P.; Perera, D.; Butaeva, E.; Lambright, S.; Castellano, F. N.; Zamkov, M. Improving the Catalytic Activity of Semiconductor Nanocrystals through Selective Domain Etching. *Nano Letters* **2013**, *13*, 2016-2023.
- (175) Wu, K.; Chen, Z.; Lv, H.; Zhu, H.; Hill, C. L.; Lian, T. Hole Removal Rate Limits Photodriven H₂ Generation Efficiency in CdS-Pt and CdSe/CdS-Pt Semiconductor Nanorod–Metal Tip Heterostructures. *Journal of the American Chemical Society* **2014**, *136*, 7708-7716.
- (176) Li, Z.-J.; Wang, J.-J.; Li, X.-B.; Fan, X.-B.; Meng, Q.-Y.; Feng, K.; Chen, B.; Tung, C.-H.; Wu, L.-Z. An Exceptional Artificial Photocatalyst, Nih-CdSe/CdS Core/Shell Hybrid, Made In Situ from CdSe

Quantum Dots and Nickel Salts for Efficient Hydrogen Evolution. *Advanced Materials* **2013**, *25*, 6613-6618.

(177) Wang, J.-J.; Li, Z.-J.; Li, X.-B.; Fan, X.-B.; Meng, Q.-Y.; Yu, S.; Li, C.-B.; Li, J.-X.; Tung, C.-H.; Wu, L.-Z. Photocatalytic Hydrogen Evolution from Glycerol and Water over Nickel-Hybrid Cadmium Sulfide Quantum Dots under Visible-Light Irradiation. *ChemSusChem* **2014**, *7*, 1468-1475.

(178) Li, Z.-J.; Li, X.-B.; Wang, J.-J.; Yu, S.; Li, C.-B.; Tung, C.-H.; Wu, L.-Z. A robust "artificial catalyst" in situ formed from CdTe QDs and inorganic cobalt salts for photocatalytic hydrogen evolution. *Energy & Environmental Science* **2013**, *6*, 465-469.

(179) Guo, Q.; Liang, F.; Gao, X.-Y.; Gan, Q.-C.; Li, X.-B.; Li, J.; Lin, Z.-S.; Tung, C.-H.; Wu, L.-Z. Metallic Co₂C: A Promising Co-catalyst To Boost Photocatalytic Hydrogen Evolution of Colloidal Quantum Dots. *ACS Catalysis* **2018**, *8*, 5890-5895.

(180) Yin, S.; Han, J.; Zou, Y.; Zhou, T.; Xu, R. A highly efficient noble metal free photocatalytic hydrogen evolution system containing MoP and CdS quantum dots. *Nanoscale* **2016**, *8*, 14438-14447.

(181) Tang, M. L.; Grauer, D. C.; Lassalle-Kaiser, B.; Yachandra, V. K.; Amirav, L.; Long, J. R.; Yano, J.; Alivisatos, A. P. Structural and Electronic Study of an Amorphous MoS₃ Hydrogen-Generation Catalyst on a Quantum-Controlled Photosensitizer. *Angewandte Chemie International Edition* **2011**, *50*, 10203-10207.

(182) Yue, D.; Qian, X.; Zhang, Z.; Kan, M.; Ren, M.; Zhao, Y. CdTe/CdS Core/Shell Quantum Dots Cocatalyzed by Sulfur Tolerant [Mo₃S₁₃]²⁻ Nanoclusters for Efficient Visible-Light-Driven Hydrogen Evolution. *ACS Sustainable Chemistry & Engineering* **2016**, *4*, 6653-6658.

(183) Simon, T.; Bouchonville, N.; Berr, M. J.; Vaneski, A.; Adrović, A.; Volbers, D.; Wyrwich, R.; Döblinger, M.; Susha, A. S.; Rogach, A. L.; Jäckel, F.; Stolarczyk, J. K.; Feldmann, J. Redox shuttle mechanism enhances photocatalytic H₂ generation on Ni-decorated CdS nanorods. *Nature Materials* **2014**, *13*, 1013.

(184) Liu, M.; Chen, Y.; Su, J.; Shi, J.; Wang, X.; Guo, L. Photocatalytic hydrogen production using twinned nanocrystals and an unanchored Ni_x co-catalyst. *Nature Energy* **2016**, *1*, 16151.

(185) Das, A.; Han, Z.; Haghghi, M. G.; Eisenberg, R. Photogeneration of hydrogen from water using CdSe nanocrystals demonstrating the importance of surface exchange. *Proceedings of the National Academy of Sciences* **2013**, *110*, 16716.

(186) Lv, H.; Ruberu, T. P. A.; Fleischauer, V. E.; Brennessel, W. W.; Neidig, M. L.; Eisenberg, R. Catalytic Light-Driven Generation of Hydrogen from Water by Iron Dithiolene Complexes. *Journal of the American Chemical Society* **2016**, *138*, 11654-11663.

(187) Qiu, F.; Han, Z.; Peterson, J. J.; Odoi, M. Y.; Sowers, K. L.; Krauss, T. D. Photocatalytic Hydrogen Generation by CdSe/CdS Nanoparticles. *Nano Letters* **2016**, *16*, 5347-5352.

(188) Ma, D.; Shi, J.-W.; Zou, Y.; Fan, Z.; Ji, X.; Niu, C.; Wang, L. Rational design of CdS@ZnO core-shell structure via atomic layer deposition for drastically enhanced photocatalytic H₂ evolution with excellent photostability. *Nano Energy* **2017**, *39*, 183-191.

(189) Wang, P.; Wang, M.; Zhang, J.; Li, C.; Xu, X.; Jin, Y. Shell Thickness Engineering Significantly Boosts the Photocatalytic H₂ Evolution Efficiency of CdS/CdSe Core/Shell Quantum Dots. *ACS Applied Materials & Interfaces* **2017**, *9*, 35712-35720.

(190) Li, W.; Lee, J. R.; Jäckel, F. Simultaneous Optimization of Colloidal Stability and Interfacial Charge Transfer Efficiency in Photocatalytic Pt/CdS Nanocrystals. *ACS Applied Materials & Interfaces* **2016**, *8*, 29434-29441.

(191) Wang, P.; Zhang, J.; He, H.; Xu, X.; Jin, Y. The important role of surface ligand on CdSe/CdS core/shell nanocrystals in affecting the efficiency of H₂ photogeneration from water. *Nanoscale* **2015**, *7*, 5767-5775.

- (192) Wang, P.; Zhang, J.; He, H.; Xu, X.; Jin, Y. Efficient visible light-driven H₂ production in water by CdS/CdSe core/shell nanocrystals and an ordinary nickel–sulfur complex. *Nanoscale* **2014**, *6*, 13470-13475.
- (193) Jana, M. K.; Gupta, U.; Rao, C. N. R. Hydrazine as a hydrogen carrier in the photocatalytic generation of H₂ using CdS quantum dots. *Dalton Transactions* **2016**, *45*, 15137-15141.
- (194) Li, Z.-J.; Fan, X.-B.; Li, X.-B.; Li, J.-X.; Zhan, F.; Tao, Y.; Zhang, X.; Kong, Q.-Y.; Zhao, N.-J.; Zhang, J.-P.; Ye, C.; Gao, Y.-J.; Wang, X.-Z.; Meng, Q.-Y.; Feng, K.; Chen, B.; Tung, C.-H.; Wu, L.-Z. Direct synthesis of all-inorganic heterostructured CdSe/CdS QDs in aqueous solution for improved photocatalytic hydrogen generation. *Journal of Materials Chemistry A* **2017**, *5*, 10365-10373.
- (195) Gimbert-Suriñach, C.; Albero, J.; Stoll, T.; Fortage, J.; Collomb, M.-N.; Deronzier, A.; Palomares, E.; Llobet, A. Efficient and Limiting Reactions in Aqueous Light-Induced Hydrogen Evolution Systems using Molecular Catalysts and Quantum Dots. *Journal of the American Chemical Society* **2014**, *136*, 7655-7661.
- (196) Brown, K. A.; Dayal, S.; Ai, X.; Rumbles, G.; King, P. W. Controlled Assembly of Hydrogenase–CdTe Nanocrystal Hybrids for Solar Hydrogen Production. *Journal of the American Chemical Society* **2010**, *132*, 9672-9680.
- (197) Utterback, J. K.; Wilker, M. B.; Brown, K. A.; King, P. W.; Eaves, J. D.; Dukovic, G. Competition between electron transfer, trapping, and recombination in CdS nanorod–hydrogenase complexes. *Physical Chemistry Chemical Physics* **2015**, *17*, 5538-5542.
- (198) Wilker, M. B.; Shinopoulos, K. E.; Brown, K. A.; Mulder, D. W.; King, P. W.; Dukovic, G. Electron Transfer Kinetics in CdS Nanorod–[FeFe]–Hydrogenase Complexes and Implications for Photochemical H₂ Generation. *J Am Chem Soc* **2014**, *136*, 4316-4324.
- (199) Wilker, M. B.; Utterback, J. K.; Greene, S.; Brown, K. A.; Mulder, D. W.; King, P. W.; Dukovic, G. Role of Surface-Capping Ligands in Photoexcited Electron Transfer between CdS Nanorods and [FeFe] Hydrogenase and the Subsequent H₂ Generation. *The Journal of Physical Chemistry C* **2018**, *122*, 741-750.
- (200) Jian, J.-X.; Liu, Q.; Li, Z.-J.; Wang, F.; Li, X.-B.; Li, C.-B.; Liu, B.; Meng, Q.-Y.; Chen, B.; Feng, K.; Tung, C.-H.; Wu, L.-Z. Chitosan confinement enhances hydrogen photogeneration from a mimic of the diiron subsite of [FeFe]–hydrogenase. *Nature Communications* **2013**, *4*, 2695.
- (201) Wu, L.-Z.; Chen, B.; Li, Z.-J.; Tung, C.-H. Enhancement of the Efficiency of Photocatalytic Reduction of Protons to Hydrogen via Molecular Assembly. *Accounts of Chemical Research* **2014**, *47*, 2177-2185.
- (202) Wang, F.; Wang, W.-G.; Wang, X.-J.; Wang, H.-Y.; Tung, C.-H.; Wu, L.-Z. A Highly Efficient Photocatalytic System for Hydrogen Production by a Robust Hydrogenase Mimic in an Aqueous Solution. *Angewandte Chemie International Edition* **2011**, *50*, 3193-3197.
- (203) Li, C.-B.; Li, Z.-J.; Yu, S.; Wang, G.-X.; Wang, F.; Meng, Q.-Y.; Chen, B.; Feng, K.; Tung, C.-H.; Wu, L.-Z. Interface-directed assembly of a simple precursor of [FeFe]–H₂ase mimics on CdSe QDs for photosynthetic hydrogen evolution in water. *Energy & Environmental Science* **2013**, *6*, 2597-2602.
- (204) Wang, F.; Liang, W.-J.; Jian, J.-X.; Li, C.-B.; Chen, B.; Tung, C.-H.; Wu, L.-Z. Exceptional Poly(acrylic acid)-Based Artificial [FeFe]–Hydrogenases for Photocatalytic H₂ Production in Water. *Angewandte Chemie International Edition* **2013**, *52*, 8134-8138.
- (205) Martinez, M. S.; Nozik, A. J.; Beard, M. C. Theoretical limits of multiple exciton generation and singlet fission tandem devices for solar water splitting. *The Journal of Chemical Physics* **2019**, *151*, 114111.
- (206) Zhang, Z.; Edme, K.; Lian, S.; Weiss, E. A. Enhancing the Rate of Quantum-Dot-Photocatalyzed Carbon–Carbon Coupling by Tuning the Composition of the Dot’s Ligand Shell. *J Am Chem Soc* **2017**, *139*, 4246-4249.

- (207) Pal, A.; Ghosh, I.; Sapra, S.; König, B. Quantum Dots in Visible-Light Photoredox Catalysis: Reductive Dehalogenations and C–H Arylation Reactions Using Aryl Bromides. *Chemistry of Materials* **2017**, *29*, 5225-5231.
- (208) Zhu, X.; Lin, Y.; San Martin, J.; Sun, Y.; Zhu, D.; Yan, Y. Lead halide perovskites for photocatalytic organic synthesis. *Nature Communications* **2019**, *10*, 2843.
- (209) Wang, K.; Lu, H.; Zhu, X.; Lin, Y.; Beard, M. C.; Yan, Y.; Chen, X. Ultrafast Reaction Mechanisms in Perovskite Based Photocatalytic C–C Coupling. *ACS Energy Lett.* **2020**, 566-571.
- (210) Wang, C.; Thompson, R. L.; Baltrus, J.; Matranga, C. Visible Light Photoreduction of CO₂ Using CdSe/Pt/TiO₂ Heterostructured Catalysts. *The Journal of Physical Chemistry Letters* **2010**, *1*, 48-53.
- (211) Sarkar, A.; Gracia-Espino, E.; Wågberg, T.; Shchukarev, A.; Mohl, M.; Rautio, A.-R.; Pitkänen, O.; Sharifi, T.; Kordas, K.; Mikkola, J.-P. Photocatalytic reduction of CO₂ with H₂O over modified TiO₂ nanofibers: Understanding the reduction pathway. *Nano Research* **2016**, *9*, 1956-1968.
- (212) Cheng, M.; Yang, S.; Chen, R.; Zhu, X.; Liao, Q.; Huang, Y. Visible light responsive CdS sensitized TiO₂ nanorod array films for efficient photocatalytic reduction of gas phase CO₂. *Molecular Catalysis* **2018**, *448*, 185-194.
- (213) Cho, H.; Kim, W. D.; Lee, K.; Lee, S.; Kang, G.-S.; Joh, H.-I.; Lee, D. C. Selectivity of photoelectrochemical CO₂ reduction modulated with electron transfer from size-tunable quantized energy states of CdSe nanocrystals. *Applied Surface Science* **2018**, *429*, 2-8.
- (214) Kuehnel, M. F.; Orchard, K. L.; Dalle, K. E.; Reisner, E. Selective Photocatalytic CO₂ Reduction in Water through Anchoring of a Molecular Ni Catalyst on CdS Nanocrystals. *Journal of the American Chemical Society* **2017**, *139*, 7217-7223.
- (215) Bi, Q.-Q.; Wang, J.-W.; Lv, J.-X.; Wang, J.; Zhang, W.; Lu, T.-B. Selective Photocatalytic CO₂ Reduction in Water by Electrostatic Assembly of CdS Nanocrystals with a Dinuclear Cobalt Catalyst. *ACS Catalysis* **2018**, *8*, 11815-11821.
- (216) Kuehnel, M. F.; Sahm, C. D.; Neri, G.; Lee, J. R.; Orchard, Katherine L.; Cowan, A. J.; Reisner, E. ZnSe quantum dots modified with a Ni(cyclam) catalyst for efficient visible-light driven CO₂ reduction in water. *Chemical Science* **2018**, *9*, 2501-2509.
- (217) Wu, H.-L.; Li, X.-B.; Tung, C.-H.; Wu, L.-Z. Semiconductor Quantum Dots: An Emerging Candidate for CO₂ Photoreduction. *Advanced Materials* **2019**, *31*, 1900709.
- (218) Lian, S.; Kodaimati, M. S.; Weiss, E. A. Photocatalytically Active Superstructures of Quantum Dots and Iron Porphyrins for Reduction of CO₂ to CO in Water. *ACS Nano* **2018**, *12*, 568-575.
- (219) Huang, J.; Gatty, M. G.; Xu, B.; Pati, P. B.; Etman, A. S.; Tian, L.; Sun, J.; Hammarström, L.; Tian, H. Covalently linking CuInS₂ quantum dots with a Re catalyst by click reaction for photocatalytic CO₂ reduction. *Dalton Transactions* **2018**, *47*, 10775-10783.
- (220) Huang, J.; Xu, B.; Tian, L.; Pati, P. B.; Etman, A. S.; Sun, J.; Hammarström, L.; Tian, H. A heavy metal-free CuInS₂ quantum dot sensitized NiO photocathode with a Re molecular catalyst for photoelectrochemical CO₂ reduction. *Chemical Communications* **2019**, *55*, 7918-7921.
- (221) Hou, J.; Cao, S.; Wu, Y.; Gao, Z.; Liang, F.; Sun, Y.; Lin, Z.; Sun, L. Inorganic Colloidal Perovskite Quantum Dots for Robust Solar CO₂ Reduction. *Chemistry – A European Journal* **2017**, *23*, 9481-9485.
- (222) Xu, Y.-F.; Yang, M.-Z.; Chen, B.-X.; Wang, X.-D.; Chen, H.-Y.; Kuang, D.-B.; Su, C.-Y. A CsPbBr₃ Perovskite Quantum Dot/Graphene Oxide Composite for Photocatalytic CO₂ Reduction. *Journal of the American Chemical Society* **2017**, *139*, 5660-5663.
- (223) Wang, Q.; Tao, L.; Jiang, X.; Wang, M.; Shen, Y. Graphene oxide wrapped CH₃NH₃PbBr₃ perovskite quantum dots hybrid for photoelectrochemical CO₂ reduction in organic solvents. *Applied Surface Science* **2019**, *465*, 607-613.

(224) Ou, M.; Tu, W.; Yin, S.; Xing, W.; Wu, S.; Wang, H.; Wan, S.; Zhong, Q.; Xu, R. Amino-Assisted Anchoring of CsPbBr₃ Perovskite Quantum Dots on Porous g-C₃N₄ for Enhanced Photocatalytic CO₂ Reduction. *Angewandte Chemie International Edition* **2018**, *57*, 13570-13574.

(225) Kong, Z.-C.; Liao, J.-F.; Dong, Y.-J.; Xu, Y.-F.; Chen, H.-Y.; Kuang, D.-B.; Su, C.-Y. Core@Shell CsPbBr₃@Zeolitic Imidazolate Framework Nanocomposite for Efficient Photocatalytic CO₂ Reduction. *ACS Energy Lett.* **2018**, *3*, 2656-2662.

(226) Brown, K. A.; Harris, D. F.; Wilker, M. B.; Rasmussen, A.; Khadka, N.; Hamby, H.; Keable, S.; Dukovic, G.; Peters, J. W.; Seefeldt, L. C.; King, P. W. Light-driven dinitrogen reduction catalyzed by a CdS:nitrogenase MoFe protein biohybrid. *Science* **2016**, *352*, 448.

(227) Bronstein, N. D.; Martinez, M. S.; Kroupa, D. M.; Vörös, M.; Lu, H.; Brawand, N. P.; Nozik, A. J.; Sellinger, A.; Galli, G.; Beard, M. C. Designing Janus Ligand Shells on PbS Quantum Dots using Ligand-Ligand Cooperativity. *ACS Nano* **2019**, *13*, 3839-3846.

(228) Kubie, L.; Martinez, M. S.; Miller, E. M.; Wheeler, L. M.; Beard, M. C. Atomically Thin Metal Sulfides. *Journal of the American Chemical Society* **2019**, *141*, 12121-12127.

(229) Kim, J.-H.; Bergren, M. R.; Park, J. C.; Adhikari, S.; Lorke, M.; Frauenheim, T.; Choe, D.-H.; Kim, B.; Choi, H.; Gregorkiewicz, T.; Lee, Y. H. Carrier multiplication in van der Waals layered transition metal dichalcogenides. *Nature Communications* **2019**, *10*, 5488.

(230) Xia, Y.; Liu, S.; Wang, K.; Yang, X.; Lian, L.; Zhang, Z.; He, J.; Liang, G.; Wang, S.; Tan, M.; Song, H.; Zhang, D.; Gao, J.; Tang, J.; Beard, M. C.; Zhang, J. Cation-Exchange Synthesis of Highly Monodisperse PbS Quantum Dots from ZnS Nanorods for Efficient Infrared Solar Cells. *Advanced Functional Materials* **2019**, *n/a*, 1907379.

(231) Xia, P.; Raulerson, E. K.; Coleman, D.; Gerke, C. S.; Mangolini, L.; Tang, M. L.; Roberts, S. T. Achieving spin-triplet exciton transfer between silicon and molecular acceptors for photon upconversion. *Nature Chemistry* **2019**.

(232) Cheng, G.-J.; Zhang, X.; Chung, L. W.; Xu, L.; Wu, Y.-D. Computational Organic Chemistry: Bridging Theory and Experiment in Establishing the Mechanisms of Chemical Reactions. *Journal of the American Chemical Society* **2015**, *137*, 1706-1725.

(233) Chen, S.; Huang, X.; Meggers, E.; Houk, K. N. Origins of Enantioselectivity in Asymmetric Radical Additions to Octahedral Chiral-at-Rhodium Enolates: A Computational Study. *Journal of the American Chemical Society* **2017**, *139*, 17902-17907.

(234) Demissie, T. B.; Hansen, J. H. Synergy between experimental and computational approaches to homogeneous photoredox catalysis. *Dalton Transactions* **2016**, *45*, 10878-10882.